

1
2
3
4
5
6
7
8
9
10
11
12
13
14
15
16
17
18
19
20

Preprint

Ice-confined construction of a large basaltic volcano –Austurfjöll massif, Askja, Iceland

Graettinger, A.H ¹; McGarvie, D. W. ²Skilling, I.P. ³; Höskuldsson, A.H. ⁴, Strand, K. ⁵

- 1University of Missouri Kansas City
- 2Lancaster University
- 3University of South Wales
- 4Haskoli Islands
- 5Thule Institute

Key words: Askja; glaciovolcanism; ice-confined; tindar; pillow lava; last glacial maximum

Corresponding author: Alison Graettinger graettingera@umkc.edu

21 **Abstract**

22 Austurfjöll is the largest basaltic glaciovolcanic massif at Askja volcano (Central Iceland),
23 and through detailed studies of its volcanological and geochemical characteristics, we provide a
24 detailed account of the sequence and structure of the ice-confined construction of a large
25 Icelandic basaltic volcano. In particular, Austurfjöll represents a geometry of vents, and resulting
26 glaciovolcanic morphology, not previously documented in ice-confined basaltic volcanoes.
27 Austurfjöll was constructed during two major phases of basaltic volcanism; via seven eruptive
28 episodes through disperse fissure-dominated eruptions. The earliest episode involved a rare
29 and poorly-exposed example of subaerial activity, and this was succeeded by six episodes
30 involving the eruption of ice-confined pillow lavas and numerous overlapping fissure eruptions of
31 phreatomagmatic tephra. Evidence of local subaerial lavas and tephra indicates the local
32 growth of eruptive centers above englacial lake levels, and subsequent flooding, but no
33 prolonged subaerial activity. Localized ice-contact facies, paleowater levels and diamictons
34 indicate the position and thickness of the ice was variable during the construction of Austurfjöll,
35 and eruptive activity likely occurred in multiple and variable level melt-water lakes during the last
36 glacial period. Lithofacies evidence including gradational transitions from effusive to explosive
37 deposits, superposition of fragmental facies above coherent facies, and drainage channels
38 suggest that changes in eruptive style were driven largely by external factors such as drainage
39 and the increasing elevation of the massif. This study emphasizes the unique character of
40 Austurfjöll, being composed of large pillow lava sheets, numerous (>40) overlapping
41 glaciovolcanic tindars and only localized emergent deposits, as a product of its prolonged ice-
42 confined eruptive history, contrasts with previous descriptions of tuyas and tindars.

43

44 **Introduction**

45 Iceland exists at the intersection of the Mid-Atlantic Ridge and the Iceland Hot Spot with
46 volcanic activity producing monogenetic volcanic constructs and long-lived central volcanoes
47 with associated fissure swarms (Einarsson 2008). Central volcanoes are large volume
48 polygenetic volcanoes constructed by repeated eruptions in a localized area and frequently are
49 characterized by bimodal volcanism (e.g. Eyjafjallajökull, Loughlin 2002; Katla, Lacasse et al.
50 2007; Krafla, Jonasson 1994). Askja is located in central Iceland and provides an opportunity to
51 investigate the repeated interaction of basaltic eruptions at a central volcano with a thick ice
52 sheet. Past work on basaltic glaciovolcanism in Iceland has concentrated on the products
53 eruptions with focused vents that have produced tuyas, tindars, or conical subglacial mounds.
54 Tuyas have distinctive flat topped and steep sided morphologies (Werner et al. 1996) and

55 tindars are linear ridges with slopes that dip away from the spine of the ridge (Schopka et al.
56 2006). These geometries dominate reviews of glaciovolcanic edifices (Hickson 2000; Komatsu
57 et al. 2007; Russell et al. 2014; Edwards et al. 2015). Only a few studies have investigated
58 polygenetic basaltic volcanoes that interacted with thick ice (Werner et al. 1996; Edwards et al.
59 2002; Smellie et al. 2008), which consequently limits our understanding of the life span,
60 frequency of eruption, and eruption styles that occur at long-lived centers under ice. Askja, in
61 central Iceland, contains multiple exposures of the internal stratigraphy of a polygenetic basaltic
62 center that interacted with thick glacial ice (Sigvaldason 1968). Askja does not have a typical
63 tuya or tindar morphology like previously described central volcanoes (Herðubreið; Werner et al.
64 1996). Askja comprises four glaciovolcanic massifs, at least three calderas, ample Holocene
65 basaltic lavas, and lesser volumes of silicic volcanic including the 1875 plinian eruption deposit
66 (Sigvaldason 1968; Carey et al. 2009; Hartley et al. 2016). This paper describes the deposits
67 and geomorphology of the Austurfjöll massif (Figure 1) that makes up the eastern wall of the
68 1875 caldera. Austurfjöll is the largest glaciovolcanic massif at Askja reaching 750 m above the
69 surrounding landscape, has an area of 48 km², and is constructed largely of pillow lava sheets,
70 pillow mounds, and overlapping fissure ridges (or tindars), that are dominantly composed
71 dominantly of glassy phreatomagmatic tephra. While these facies are typical of basaltic
72 eruptions into ice-confined lakes, the topography of the massif steps down in a series of ridges
73 and valleys towards the east, away from the caldera rim, representing repeated basaltic
74 eruptions in multiple and variable volume ice-confined lakes.

75 Austurfjöll was investigated using a combination of field-based lithofacies descriptions,
76 geomorphology, and geochemical data. The degree of preservation, a lack of major erosional
77 surfaces, and an absence of extensive glacial diamictite deposits suggests that Austurfjöll was
78 produced during the last (Weichselian) glacial period. Detailed lithofacies analysis shows the
79 dominance of ice-confined fissure eruptions of phreatomagmatic tephra over extensive pillow
80 lava sheets, the collapse of unstable edifices, and subsequent transport and deposition of
81 material in water. Local deposits of subaerially emplaced pyroclastic deposits and lava flows
82 reveal the variable nature of the water level within ice-confined lakes. Intrusions are a common
83 feature in coherent and fragmental lithofacies and provide additional evidence about the
84 emplacement environment. The recognition of seven eruptive units, through stratigraphic
85 relationships including two diamictite units supported by geochemical trends, indicates that the
86 construction of Austurfjöll involved multiple ice-confined eruptions and vents in multiple lakes.
87 This growth model introduces a new level of complexity to the way that large long-lived basaltic
88 volcanoes grow in the presence of thick ice sheets. This model has implications for the stability

89 of an ice sheet over a productive volcanic edifice without a centralized vent, such as the
90 presence of multiple meltwater lakes that can vary in size and distribution through time and
91 erosive drainage events (Smellie 2006). Furthermore, this newly described morphology is
92 relevant for studies of glaciovolcanic constructs on Mars that are dependent on terrestrial
93 analogs and topographic data (Ghatan and Head 2002; Houvis et al. 2008; Martinez-Alonso et
94 al. 2011).

95

96 **Methods**

97 Field work focused on lithofacies descriptions, structural measurements, and sample
98 collection, and was supplemented by ground and aerial-based photographic documentation.
99 Lithofacies descriptions include bed thickness, sedimentary structures and contacts, clast type,
100 clast shape and clast size as documented in the field and supplemented by observation of
101 samples. The partially lithified nature of the deposits throughout the massif precluded the use of
102 traditional granulometric analyses. Consequently, maximum and median clast sizes were
103 manually measured in the field and corroborated with photographs. Vesicularity was visually
104 estimated in the field and from thin sections using ImageJ.

105 The distribution of lithofacies was mapped using available exposures and stratigraphic
106 logs, and then extrapolated to areas of poor/zero exposure and where access was difficult (e.g.
107 along the actively collapsing caldera wall) (Graettinger et al. 2013a). Twenty-three stratigraphic
108 logs were drafted and these were used to reconstruct the relationships between lithofacies and
109 to document stratigraphic and erosional boundaries within Austurfjöll (Figure 1). Most logs were
110 collected in steep-sided gullies. An additional 19 logs collected by Strand and Höskuldsson in
111 1980 for NORVOLK (Strand 1987) around the caldera rim were used to supplement the new
112 logs.

113 Bulk rock geochemical analyses of 57 rock samples were conducted using X-Ray
114 Fluorescence spectroscopy (XRF) at McGill University (Montreal, Canada) and Washington
115 State University GeoAnalytical Lab (Pullman, USA). Samples analyzed were from coherent
116 facies including pillowed and non-pillowed lavas, intrusions, and lava clasts within fragmental
117 units within recognized stratigraphic units as part of a complete facies characterization (Cas and
118 Wright 1987). Samples with visible alteration or zeolites were avoided. Repeat analyses of
119 samples from a single stratigraphic unit were used to establish the variability of unit chemistry.
120 Once established, the geochemical signatures were used to aid stratigraphic correlation of
121 eruptive products that were not laterally continuous and map these units across the massif.

122

123 **Lithofacies**

124 Glaciovolcanic lithofacies were divided into ash tuff, lapilli tuff, breccia, and lavas.
125 Subdivisions of these lithofacies were based on componentry and sorting. Macro-phenocrysts of
126 plagioclase are common in some deposits and are noted as a characteristic trait for
127 identification in the field (an x is added to the lithofacies code), but as porphyritic units do not
128 otherwise vary from similar lithofacies lacking crystals they are not discussed separately (Table
129 1).

130

131 *Lavas*

132 Coherent lithofacies (lavas) are divided into pillowed and non-pillowed groups, and
133 interpreted to be subaqueous or subaerial based on internal and surface textures. Pillowed
134 lavas are far more common than non-pillowed lavas, and were subdivided into two facies based
135 on the size and regularity of the stacking of pillow lava tubes. Regular pillows (PI1) range in size
136 from 10-50 cm in cross-sectional diameter with elliptical shapes. The similarity in pillow
137 diameters results in organized stacking of pillow tubes. Irregular pillow lavas (PI2) range in size
138 from 5-200 cm in cross-sectional diameter, which produces irregular stacking of pillow shapes
139 interspersed with local zones of columnar or entablature jointing between pillow tubes. Vertical
140 pillows and mega-pillows (≥ 200 cm in cross-section) are observed locally in irregular pillow
141 lavas.

142 Non-pillowed lavas occur in small outcrops with extents no greater than a few tens of
143 meters and they are assigned to two groups: vesicular entablature-jointed lavas (L1) and dense
144 reddened lavas with locally scoured scoriaceous tops (L2). L1 lavas can transition laterally into
145 PI1 pillowed lavas. Some L1 lavas exhibit radial fractures that extend through the flow. L2 lavas
146 have a distinct red coloration and locally present scoriaceous tops and/or surface scours. In thin
147 section, the L2 lavas have an abundance of oxide microlites absent in all other facies.

148

149 *Interpretation*

150 The bulk of lavas observed at Austurfjöll (PI1, PI2 and L1) have characteristics typical of
151 subaqueous lavas such as pillow morphologies, entablature fracturing, and/or thick chill rinds
152 (Dimroth et al. 1978; Gregg and Fink 1995; Smellie and Hole 1997; Kennish and Lutz 1998;
153 Goto and McPhie 2004; Tucker and Scott 2009). Pillow lavas (PI1 and PI2) represent a low
154 effusion rate whereas sheet lavas (L1) represent higher effusion rates (Gregg and Fink 1995;
155 Parfitt et al. 2002; Gregg and Smith 2003). There is no correlation between phenocryst
156 abundance and lithofacies assignment (PI1, PI2), and field estimates of vesicularity varies

157 between 30-70% for both facies. Both pillow facies occur at multiple locations around the
158 massif, at variable distances to candidate vents, and can be traced laterally for tens of meters,
159 suggesting this difference is not simply controlled by distance from a vent. Rather, we suggest,
160 the changes in pillow lava morphology at Austurfjöll are dependent on the lava-supply rate, and
161 not variations in viscosity due to cooling (Walker 1992). As such, the irregularity of PI2 lavas are
162 interpreted to represent an end-member of pillow style effusion, where a minor increase in
163 eruption rate results in the development of textures transitional to lobate flows, such as larger
164 lobes, and presence of entablature jointing. L2 non-pillowed lavas are interpreted to be
165 subaerial in origin, showing significant evidence of interaction with oxygen (oxide microlites and
166 red color). Where present, the local scoriaceous top implies that the flows had a'a structures
167 and were likely eroded by glacial activity that removed the top and produced observed scours.

168

169 *Breccias and diamictites*

170 Breccias and diamictites are common at Austurfjöll and are differentiated by clast type
171 and shape as well as sorting. This lithofacies include pillow and fluidal bomb breccias (B1),
172 angular block breccias (B2), red lava fragment-bearing breccias (B3), and glacial clast-bearing
173 diamictites (Dia1 and Dia2). Deposit color is influenced by the abundance and degree of
174 palagonitization of ash-sized matrix material.

175

176 *Breccias*

177 Pillow and fluidal bomb bearing breccias (B1) are typically clast-supported with clasts 7-
178 70 cm in diameter, and contain recognizable pillow forms, pillow fragments, and/or fluidal bombs
179 (Figure 2a). Some clasts have distinctive glassy rims 2-10 mm thick. There is no regular
180 structure to these deposits, and they can transition laterally and vertically into pillow lavas (PI1
181 and PI2). The matrix is dominated by lapilli-sized angular vitric particles with local
182 concentrations of coarse ash. Vesicularity of the lapilli (from visual estimates) is variable, but is
183 typically between 10-30% in hand samples and thin sections. Pillow breccias (B1) are often cut
184 by dikes of various morphologies.

185 Angular block-bearing breccias (B2) are clast- to variably matrix-supported (Figure 2b).
186 These breccias display zones of clast concentrations, but not bedding. Clast size and matrix
187 variation in angular breccias are similar to B1 breccias, but the clast shapes are notably angular.
188 Red lava fragment breccias (B3) occur typically in thin (<1 m) lenses between lapilli tuffs and
189 subaerial lavas along the caldera rim. B3 breccias contain distinctive clasts of dense red-hued
190 lava (L2) and red scoria. Other clasts in B3 breccias include microcrystalline lava, porphyritic

191 lava, and lithified ash tuff. B3 breccias are clast- or matrix-supported. The breccia matrix
192 consists of coarse ash and lapilli, with a wide range of vesicularities and particle shapes.

193

194 *Interpretation*

195 Breccias are a common feature in glaciovolcanic settings and are produced in a variety
196 of eruptive and post-eruptive conditions. There are many mechanisms for producing clast-
197 supported breccias, including: collapse, flow-generated breccias, explosion, and disruption by
198 intrusions (peperite formation or destabilization; Carlisle 1963; Dimroth et al. 1978; Loughlin
199 2002; Sansone and Smith 2006; Vezzoli et al. 2008; Edwards et al. 2009; Skilling 2009; Tucker
200 and Scott 2009; Mercurio 2011; Kralj 2012; Watton et al. 2013). The nature of the clasts in
201 conjunction with field relationships helps differentiate between breccias formed by either
202 explosive, intrusive, or gravity-driven processes. Breccias at Austurfjöll (B1, B2, and B3) show
203 similar textural characteristics in terms of clast-support, clast size range, and deposit thickness,
204 but each facies has distinct clast types. B1 breccias contain unequivocal clasts of intact and
205 fractured pillows and in some cases fluidal bombs, and therefore contain primary or only slightly
206 reworked eruptive products. They are interpreted to be the result of explosive processes near or
207 through pillowed lavas, and/or the collapse of pillowed lava flow margins. In contrast, B2 and B3
208 are associated with angular blocks that may be of ballistic, but more commonly, gravitational
209 origin. Blocks in B3 are interpreted as fragments of broken subaerial lava (L2), with oxidation
210 staining and occasional scoriaceous textures. B1 and B2 breccias are associated with pillowed
211 and non-pillowed lavas at a range of elevations. B3 breccias occur predominantly at higher
212 elevations along the caldera rim and outward directed dips indicate that the breccias likely have
213 a source somewhere in what is now the caldera.

214

215 *Diamictites*

216 Two diamictite lithofacies occur at Austurfjöll. Rounded cobble diamictite (Dia1) is
217 moderately lithified and contains diverse clast lithologies that are well-rounded with scoured and
218 polished surfaces. The clasts are supported by a grey-brown fine ash matrix, distinct from
219 breccia matrix in both color and dominance of sand and silt sized material (Figure 2c). The
220 deposit is poorly-sorted and is massive in structure. Outsized clasts and matrix components
221 both include low to highly vesicular clasts of lava with variable crystal populations. Clasts of
222 palagonitized tuff are rare, and where present are pebble-sized or smaller. Deposits of Dia1 are
223 typically on the order of one meter thick, and do not occur in beds or have consistent contacts.

224 This lithofacies is not laterally continuous beyond a few meters, locally mantles vertical
225 exposures, and is disrupted by pillowed intrusions.

226 Matrix-supported pebble diamictite (Dia2) has centimeter-scale bedding and contains
227 subrounded to rounded clasts supported in a grey-brown fine ash matrix (Figure 2d). Clasts are
228 typically small cobble to pebble-sized and may display glacial polish or striations. Outsized
229 clasts are diverse, but dominant clast types include dense and vesicular lava. The diamictite is
230 typically on the order 50 cm or less in thickness, and has a sub-horizontal upper surface that
231 may extend several hundred meters along the southeastern margin of Austurfjöll. The Dia2
232 lithofacies overlies lavas exhibiting glacial scour.

233

234 *Interpretation*

235 Dia1 is a massive deposit that contains clasts with distinctive glacial signatures, such as
236 surface scours. The concentration of glacially altered clasts, sorting, and massive nature
237 indicates that the deposit is either glacial in origin or reworked from a glacial deposit.

238 Descriptions of glacial deposits at glaciovolcanic centers are limited (Bergh and Sigvaldason
239 1991; Loughlin 2002; Bennett et al. 2006; Smellie 2008; Carrivick et al. 2009) partly because the
240 lithologies available for incorporation into diamicts are so similar in Iceland. The lack of lateral
241 continuity of the deposits described at Austurfjöll suggests that these deposits are not regional-
242 scale glacial till deposits, but either localized lodgment tills, moraine deposits, or related to
243 subglacial fluvial transport. The extent of these deposits is difficult to constrain due to incision of
244 younger gullies. Some of the Dia1 deposits are also disrupted by intrusions and/or loading from
245 overburden. Intrusions with convolute morphologies into Dia1 indicate volcanic activity resumed,
246 or was active, when deposits were unconsolidated. Intrusions and stratigraphic relationships
247 suggest Dia1 deposits were emplaced before and between the first two pillow lava eruptive units
248 at Austurfjöll. The more continuous distribution, finer grain size and bedding of Dia2 suggest
249 that they are localized glacial outwash deposits, where the glacially deposited material was
250 fluvially remobilized by meltwater at the base or front of the glacier. The narrow distribution of
251 diamictite deposits between subaqueous eruptive deposits, suggests that the diamictites do not
252 represent a prolonged hiatus in eruptive activity.

253

254 *Lapilli and Ash tuff*

255 The most voluminous lithofacies at Austurfjöll are the ash and lapilli tuffs, making up
256 almost 50% of the total massif volume. These are distinguished from each other by clast
257 morphology and componentry. Deposit color is influenced by the abundance and degree of

258 palagonitization of ash-sized material. Angular vitric lapilli tuff (Lt1) is massive and can display
259 variable amounts of matrix palagonitization. Occasional fluidal bombs reach up to 50 cm in
260 diameter (Figure 3a). The deposit is poorly sorted and lapilli-supported, with occasional fine ash
261 matrix, and can display a weak upward fining. These deposits are described and interpreted in
262 detail in Graettinger et al. (2013b). Subrounded lapilli tuff (Lt2) contains distinctive subrounded
263 blocks in a lapilli-dominated matrix. Lapilli are 1-6 cm in diameter. Blocks are sub-angular to
264 rounded and up to 30 cm in diameter. Typical blocks include vesicular to non-vesicular rounded
265 lava that can occur in concentration zones of, but with no regular bedding. The facies is
266 otherwise poorly sorted (Figure 3b). Red scoria lapilli tuff (Lt3) contains subrounded lapilli with
267 distinctive clasts including red scoria and armored lapilli (Figure 3c). The deposit is clast- or
268 matrix-supported with outsized clasts of bombs/bomb fragments. Lt3 is the only lapilli facies to
269 contain rare bomb sags. Heterolithic lapilli tuff (Lt4) facies contains little to no fresh glass in a
270 highly heterolithic subrounded to rounded lapilli-dominated tuff. Clast composition includes
271 dense and vesicular lavas, red scoria, and consolidated blocks of ash tuff. The deposit is
272 supported by a coarse ash matrix. Blocks are up to 20 cm in diameter (Figure 3d).

273 Massive coarse ash tuff (At1) is composed of predominantly coarse ash and forms beds
274 that are frequently thick (>5-50 m), displaying occasional blocks of lava fragments. Thin
275 localized zones of weakly bedded material are uncommon (Figure 4a). Bedded to laminated
276 ash tuff (At2) contains coarse ash, fine ash, and occasional very fine ash beds that are well-
277 sorted. Laminations occur on the scale of <2 cm within beds having a maximum thickness of 2
278 m. Occasional millimeter- to centimeter-thick very fine ash layers occur (Figure 4b). Alternating
279 bedded ash tuff (At3) consists of well-sorted coarse ash beds of 5-50 cm thick, that are inter-
280 bedded with fine ash beds of 3-15 cm thick. Weak centimeter-scale sedimentary structures such
281 as cross-bedding, ripple marks, and normal grading also occur. Overall At3 deposit thickness
282 can vary from a few centimeters to >15 m thick (Figure 4).

283 Highly deformed domains, or packets, of vitric ash to lapilli tuff (At4) are a common
284 feature in the field area. These domains occur at all elevations, and overlap all other lithologies.
285 At4 deposits comprise domains of coarse ash-dominated, bedded sediment that display both
286 meter-scale folding and centimeter-scale convolutions (Figure 5). These deformed sediment
287 domains display preserved internal bedding, lamination, and sedimentary structures (including
288 scours, cross-bedding, and ripples), but the packets of sediment in most cases display a steeply
289 dipping orientation and are folded at high angles (tilted bedding is as high as 85⁰). Individual
290 beds are centimeters thick (5-10 cm average), with varying clast sizes from fine ash, to coarse
291 ash, and lapilli up to 4 cm. Clasts vary from subrounded to rounded lapilli, to <10 cm diameter

292 angular blocks of dense to vesicular lava. Packets of At4 range from 20-200 cm thick. Contacts
293 with surrounding beds are typically very sharp, but transitional boundaries with undeformed
294 beds of At2 and At3 are observed.

295

296 *Interpretation*

297 The Austurfjöll ash and lapilli tuff deposits are dominated by Lt2 and At1 facies. These
298 two lithofacies are dominated by subrounded to subangular, poor to moderately sorted particles
299 that may be weakly bedded or massive. The rounding of clasts and, more importantly, the
300 development of local sedimentary structures is indicative of transport in water following eruption.
301 Bedding, cross-stratification, ripple marks, and loading structures are most common in the ash-
302 dominated facies. Lapilli tuffs with poor sorting and lack of sedimentary structures represent
303 rapid deposition of large volumes of highly-concentrated material (Maicher et al. 2000). The
304 occurrence of increased bedding and traction current structures in more distal ash tuff deposits
305 (At2) is consistent with sediment gravity flows described from subaqueous eruptive centers
306 (White 2000). Subaqueous density current deposits dominate the deposits of other
307 glaciovolcanic and submarine volcanic centers (Maicher et al. 2000; White 2000; Schopka et al.
308 2006) and are considered the likely mechanism of emplacement for these facies. Thick (20 m)
309 and massive deposits such as At1 may represent deposits that were rapidly emplaced without
310 significant remobilization. However, palagonitization, a common process in vitric basaltic
311 deposits, can mask evidence of bedding or other fine structures - particularly in ash-dominated
312 deposits (Stroncik and Schmincke 2002). This is observed in partially palagonitized ash-
313 dominated deposits at Austurfjöll. The Lt1 facies is the only example of primary subaqueous fall
314 out, or direct settling of pyroclastic material from an explosion of coarse material, identified at
315 Austurfjöll. These deposits are distinguished by a high degree of angularity of all grain sizes,
316 preserved fragile glassy particles, a gradational upward fining, and fluidal bombs (Graettinger et
317 al. 2013b).

318 The steep slopes of unconsolidated deposits that comprise glaciovolcanic piles are
319 conducive to collapse, and can produce deposits with similar characteristics to eruption-fed
320 density currents (Sansone and Smith 2006). The regular bedding and frequent presence of
321 sedimentary structures such as ripples and loading structures within At2 and At3 are indicative
322 of either low energy density currents (distal flows of eruption-fed currents) or the gravitational
323 remobilization of previous deposits. Distinguishing between these deposits depends on slope
324 and stratigraphic relationships. Measured slopes of At2 and At3 deposits are typically between
325 10° and 25° . Deposits at steeper angles (ca. 20°) likely indicate distal deposits of eruption-fed

326 density currents that were not remobilized. At2 deposits on shallower slopes most commonly
327 occur in large packets up to 40 m thick and fill large (100 m wide) channel forms, suggesting a
328 remobilized history. This indicates that there was significant remobilization of deposits at
329 Austurfjöll.

330 Lt3 and Lt4 facies contain more diverse components than Lt1-2 and At1-3, and have a
331 limited distribution along the margin of the caldera at high elevations (Figure 1) with dips that
332 radiate away from the caldera rim. These facies sometimes contain subaerially-derived clasts
333 such as red scoria and blocks of subaerial lava. Lt3 contains armored lapilli, which likely formed
334 above the water level, and could be emplaced subaerially or in calm and shallow subaqueous
335 environments (McPhie et al. 1993; White 1996). Additional support for a shallow water
336 interpretation occurs in rare bomb sags in this lithofacies. The Lt3 facies is, therefore,
337 interpreted as an indicator of shallow or subaerially-emplaced emergent deposits. Lt4 contains a
338 combination of subaerially- and subaqueously-derived clasts, suggesting the remobilization of
339 subaerial deposits in an erosive traction current or through collapse to incorporate both clast
340 types. The dominance of these facies along the caldera rim suggests a lake level near this
341 elevation. Further evidence of such a lake level has been lost to the caldera subsidence event
342 that removed the westernmost sector of the Austurfjöll glaciovolcanic massif.

343 Deformed domains of At4 occur at multiple elevations on all other lithofacies at
344 Austurfjöll. The fairly fine (centimeter-scale) bedding of the domains, including ripples and
345 channel forms, indicate that they are likely the result of small subaqueous gravity flows. The
346 modern steep angles and deformation of these deposits suggests partial collapse of the
347 underlying deposits, or slumping at the margin of pillow lava flows or sediment piles. The
348 preservation of both sharp contacts and local transitions into undisturbed beds supports a
349 collapse origin for the deformation. The commonality of these features only further underline the
350 instability of growing piles of volcanic deposits within ice-confined lakes.

351

352 *Intrusions*

353 Intrusions are common in glaciovolcanic complexes, and Austurfjöll is no exception.
354 Basaltic dikes intrude both pillowed and fragmental host materials. Dike morphologies vary from
355 narrow tabular dikes of 50 cm in diameter to complicated pillowed dikes and coherent margined
356 volcanoclastic dikes (CMVD) 1 to 3 m in diameter (Graettinger et al. 2012). Intrusions were
357 frequently found at the center of linear tindar ridges composed of fragmental material with
358 peperite or sharp contacts with the host material.

359

360 *Interpretation*

361 The pillowed, convolute, and tabular intrusions observed at Austurfjöll are similar to
362 those described in other glaciovolcanic centers (Edwards et al. 2009; Skilling 2009). The dike
363 morphologies provide important information about the environments at the time of their
364 emplacement (Schopka et al. 2006; Edwards et al. 2009; Stevenson et al. 2009). Tabular dikes
365 are typical of basaltic volcanic centers where magma interacts with competent rock and lithified
366 deposits (Baer 1995; Rivalta and Dahm 2006). These dikes can serve as feeders for eruptions,
367 or they may be arrested on the way to the surface. Pillowed dikes and peperitic margins are
368 indicative of intrusion into unconsolidated, and typically wet, sediments (Walker 1992; Doyle
369 2000; White et al. 2000; Skilling et al. 2002; Mercurio 2011). CMVDs are interpreted as the
370 result of magma interacting with ice-cemented sediments (Graettinger et al. 2012), and although
371 they have not yet been described at other tuyas or tindars, they are expected to be common in
372 ice-confined volcanic centers.

373

374 **Lithofacies associations**

375 The bulk of Austurfjöll is composed of coherent and fragmental deposits erupted in
376 contact with water and ice. The rarity of subaerial deposits indicates that abundant water was
377 present in ice-confined lakes during the construction of Austurfjöll. The facies associations can
378 be grouped into three major constructs: tindars, thick pillowed lava flow sheets, and pillow
379 mounds. Depositional centers of reworked material occur between these constructional
380 features. The constructive lithofacies are typically ordered into localized sequences of pillow
381 lava and pillow breccia (PI1, PI2, B1) or subaqueous lavas and related breccias (L1, B2),
382 overlain by fragmental deposits of ash and lapilli tuffs (Lt1, Lt2, At1) (Figure 6). Roughly,
383 Austurfjöll is composed of large pillow lava sheets overlain by stacked and overlapping tindars,
384 with local pillow mounds. Deposits of remobilized fragmental material accumulate in topographic
385 lows and as channel fills between eruptive vents (At2, At3, At4). Many of the depo-centers are
386 cross-cut by dikes, indicating that intrusion, primary and reworked deposition were all broadly
387 contemporaneous.

388

389 *Tindars*

390 The most common eruptive construct exposed on Austurfjöll are glaciovolcanic fissure
391 ridges, also known as tindars. Tindars are linear ridges composed of fragmental volcanic
392 material with slopes that dip away from the spine of the ridge. These tindars are distinguished
393 from tuff cones as they do not present quaquaversal (circular radially outward dipping)

394 structures and instead are linear features with beds dipping away from the ridge axis. The linear
395 ridge of fragmental deposits with an intrusive core is typical of tindars described from numerous
396 locations in Iceland and British Columbia (Werner and Schmincke 1999; Schopka et al. 2006;
397 Edwards et al. 2009; Jakobsson and Gudmundsson 2008; Mercurio 2011; Pollock et al. 2014).
398 Tindars have also been described composed predominantly of pillow lavas, but presenting a
399 linear morphology (Werner and Schmincke 1999; Höskuldsson et al. 2006; Edwards et al. 2009;
400 Pollock et al. 2014). Austurfjöll tindars are composed predominantly of ash and lapilli tuffs (Lt1,
401 At1, Lt2, At2) and are, in most cases, cored with a feeder dike that may have a tabular and/or
402 pillowed morphology (Figure 7a). In some tindars, basal pillow lavas and pillow breccias are
403 partially exposed. Unlike the isolated tindars that occur in fissure swarms around Iceland,
404 Austurfjöll tindars occur in close proximity and overlap each other. Tindars at Austurfjöll are
405 typically 300 m in length and 50 m high relative to surrounding terrain. Typical fissure swarm
406 tindars have a length of twice the width of the ridge (Jakobsson and Gudmundsson 2008), and
407 these same proportions apply to most Austurfjöll tindars. Additionally, the Austurfjöll tindars
408 occur in large numbers and are constructed predominantly on top of previous eruptive
409 constructs. This study has identified over 40 individual tindars currently exposed at Austurfjöll,
410 with an unknown number of buried tindars (Figure 8). The presence of numerous closely spaced
411 and locally overlapping tindars produces the prominent stepped appearance of Austurfjöll. This
412 is augmented by the infill of topographic lows between ridges by primary and remobilized ash
413 and lapilli tuffs. Some of the inter-tindar depo-centers contain large channel structures up to 100
414 m across, suggesting that the deposits were eroded rapidly during and/or soon after their
415 formation (Figure 7b).

416

417 *Pillow lava sheet*

418 Pillow lava sheets form the base of Austurfjöll and are only exposed at low elevations,
419 particularly along the southeastern sector (Figure 1). The sheets can extend up to 1 km in
420 length with individual sheets up to 60 m thick and typically have distinctive sub-horizontal tops
421 (Figure 7c). Exposed interiors of these sheets indicate they are composite and comprise
422 multiple pillowed lava flows, with local marginal breccias (B2). Individual flows within a pillow
423 lava sheet can be made up of PI1 or PI2 lavas and local lobate lava flows (L1). These three
424 facies can show either gradual transitions or sharp contacts. Pillow lava sheets may be stacked,
425 with pervasive sub-horizontal contacts typically associated with a change between PI1 and PI2
426 facies. A few examples of vertical pillows at the contact between individual flows suggest that
427 the pillow lava sheets may have locally interacted with the confining ice, or a thin meltwater lens

428 between the flow front and the ice (Hungerford et al. 2014). Steep-sided gullies incised into the
429 southeastern sector reveal that stacked pillow lava sheets are up to 100 m thick. The plateaus
430 associated with the top of pillow lava sheets are buried by overlapping tindars and less common
431 pillow mounds. No vents for the pillow lava sheets are exposed, but the dominance of fissure-
432 controlled geometries at Austurfjöll (Figure 8) suggests that they may have also been fissure-
433 fed.

434

435 *Pillow mounds*

436 Pillow mounds are less common but widespread, and are generally no more than a few
437 tens of meters in size and 15-30 m thick. They occur stratigraphically above the major pillow
438 lava sheets and form steep slopes between 40-50 degrees (Figure 7d). These mounds are
439 constructed of PI1 or PI2 facies pillowed lava flows. The bases of the mounds are frequently
440 buried by local detritus and/or pyroclastic deposits from the AD 1875 eruption. The pillow
441 mounds typically occur on shallow slopes of ~10 degrees. Pillow mounds occur either as
442 clusters, or as a single mound and display circular footprints. These constructs reflect entirely
443 effusive subaqueous eruption histories, and are limited in size at Austurfjöll to a few tens of
444 meters in diameter. These features contrast with conical features composed of predominantly
445 pillows and interstitial breccias and tuff, referred to as subglacial mounds described up to 2 km
446 in diameter in British Columbia, Canada (Hickson 2000). The size limitation at Askja may be
447 related to the abundance of fissure-type vents, rather than a focused vent.

448

449 *Subaerial deposits*

450 The lowest stratigraphic deposits exposed at Austurfjöll are glacially scoured subaerial
451 lavas. The lavas have limited exposures, but appear to be laterally extensive (~30 km²). All
452 other subaerial deposits occur only locally, most frequently as clastic deposits containing
453 subaerial components (i.e. B3, Lt3, Lt4). Pyroclastic (Lt3) and effusive (L2) deposits occur
454 around the caldera rim at elevations greater than 600 m above the local base level (1250-1450
455 m asl) representing the highest preserved modern elevations of Austurfjöll (Figure 1). These
456 deposits are surrounded by subaerial clast-bearing breccias and tuffs (B3, Lt4) that suggest the
457 primary subaerial deposits were emergent and partially remobilized down slope to be deposited
458 in shallow water. The only examples of bomb sags at Austurfjöll occur in these remobilized
459 deposits near the caldera rim. As these features occur in the absence of confining topography,
460 they likely represent a maximum ice-confined water level during late stage construction of
461 Austurfjöll.

462 Three other locations of subaerial deposits were found on Austurfjöll and are
463 interbedded with subaqueous deposits. These isolated subaerial lavas occur at lower elevations
464 and cover less than 1 km² each. These lavas occur at roughly 560-600 m above the local base
465 (1160-1200 m asl) and occur in the NW, NE and SE sectors of Austurfjöll (Figure 6). These
466 lavas probably indicate fluctuations in the levels of ice-confined lakes during the construction of
467 Austurfjöll. These fluctuations may be associated with temporary drainage, or emergence of
468 eruptive vents. Both scenarios require a subsequent increase in lake level to produce
469 subaqueous lavas on top of the subaerial lavas and serve to illustrate the typically dynamic
470 nature of water levels during construction of glaciovolcanic edifices (Skilling, 2009).

471

472 *Glacial and fluvial deposits*

473 Local matrix-supported diamictites containing glacially polished clasts are interpreted as
474 either local glacial tills or locally reworked till material. Local interaction with ice (till, vertical
475 pillows, radial cooling cracks on lavas, glacial scour and glacial erratics) indicates that the ice
476 margin was at times close to, or covering some of the eruptive deposits. The glacial deposits,
477 however, do not form extensive horizons that would indicate a prolonged hiatus between
478 eruptive events, or major recursions of ice over the massif, suggesting that Austurfjöll was likely
479 constructed entirely during the last glacial period (Weichselian).

480 Fluvial deposits are located predominantly in depositional centers between tinar ridges
481 and pillow mounds. The At2 and At3 facies are interpreted as reworked material from
482 subaqueous eruptions because of their dominance of sedimentary structures and low angle
483 bedding. The eruption of fine-grained material onto steep slopes in a subaqueous environment
484 is conducive to remobilization. Rare examples of large drainage channels suggest that the
485 volume of water within the ice-confined environment may have changed rapidly and reworked
486 large volumes of sediment quickly (Figure 7b). The occurrence of localized subaerial deposits at
487 lower elevations in the massif that transition laterally into subaqueous deposits support falling
488 lake levels (Smellie 2006; Russell et al. 2013)

489

490 **Geochemical Data**

491 Whole rock geochemistry of 54 volcanic rocks from Austurfjöll lavas, dikes, and blocks
492 from fragmental deposits (Pl, L, B, Dia, and Lt) was undertaken. The purpose was to determine
493 the compositions of erupted melts produced during the construction of Austurfjöll to provide
494 insight into the range of compositions produced during pre-Holocene period. The geochemistry

495 was also leveraged to support stratigraphic relationships where physical connections between
496 eruptive units was either lacking or obscured, a common issue in glaciovolcanism.

497 All 54 volcanic rocks analyzed are basalts on the basis of SiO₂ contents (i.e. 48-52%;
498 Figure 9), and normative mineralogy indicates that these basalts are tholeiites, with 21 being
499 quartz tholeiites and 33 being olivine tholeiites. Similar basalt compositions have been reported
500 for Holocene basalts at Askja (Macdonald et al., 1987; Kuritani et al., 2011). The common
501 occurrence of quartz tholeiites at Icelandic central volcanoes located in the active rift zones has
502 long been recognized (Wood, 1976, 1978), where slightly more evolved melts are generated in
503 comparison to the offshore spreading segments of the Mid-Atlantic Ridge.

504 The geochemical characteristic of the erupted basalt was also used as means of
505 corroborating the primary stratigraphy of Austurfjöll based on field mapping. The geochemical
506 character of eruptive units was established by first grouping stratigraphically known samples,
507 and then evaluating the variability within each unit. This ensured that the primary stratigraphy,
508 established by field mapping, took precedence. Once established, the geochemical signatures
509 were then used to correlate eruptive products that are not laterally continuous (Figure 9) and
510 map these eruptive units across the massif (Figure 10).

511 To test this, 23 samples from a single and extensive pillow lava sheet (Unit 2) were
512 analyzed, and the results are shown in Table 2, where the variability of Nb (17-20 ppm) and Y
513 (34-42 ppm) are small, whereas the ranges for Rb (2-14 ppm), Zr (150-172 ppm) and Ce (31-57
514 ppm) are greater. Note also that the ratios of incompatible trace elements show similarly low
515 variability, with Y/Nb, for example, varying from 1.8 to 2.5, with 21 of the 23 samples lying in the
516 range 1.9-2.2. Similar relationships are seen in Rb/Nb and Zr/Nb ratios, with the bulk of
517 analyses lying within a restricted range (Table 2). This process established that 23 samples
518 from one well-defined eruptive unit possess a suitably narrow range of compositions to enable
519 the correlation of stratigraphic units when physical connections were missing or obscured.
520 Samples whose stratigraphic relationships were uncertain were then assigned to one of the
521 Units by matching their trace element characteristics to a specific Unit. This proved to be
522 relatively straightforward to do, as each Unit was observed to have its own subtle but distinctive
523 geochemical characteristics, most clearly expressed in the relative concentrations of the trace
524 elements Nb, Rb, Y, Zr, and Ce (Table 3). The relative enrichment of these six incompatible
525 elements shows the distinctive signature of the units (Unit 6<Unit5<Unit4<Unit1<Unit2
526 <Unit3<Unit7). The complete dataset is available as Online Resource 1.

527 This supplementary geochemical corroboration enabled a refined eruptive history of
528 Austurfjöll that reinforced field observations including the large extent of pillow lava sheets (Unit

529 2) and the limited extent of some eruptive units (Unit 4 and 7). Additionally, this process
530 revealed the presence of Unit 2 clasts within diamict (Dm2) enhancing the rich stratigraphic
531 story preserved at Austurfjöll.

532

533 **Eruptive history of Austurfjöll**

534 The stratigraphically lowest unit of Austurfjöll occurs at an elevation of 600 m asl and
535 comprises glacially scoured subaerial a'a lavas (Unit 1). There is a locally exposed erosional
536 boundary between the Unit 1 subaerial lavas and the overlying glacial diamictite (Dm 1), which
537 is overlain by the first pillow lavas (Unit 2). Basaltic activity occurred while the glacial deposits
538 were still unconsolidated as there are complex intrusions and peperites cross-cutting the
539 diamictites. The earliest glaciovolcanic activity at Austurfjöll involved the formation of Unit 2,
540 which is a ca 10 km² and 1 km³ pillow lava sheet covered by tindars and remobilized tuff. The
541 fragmental deposits were emplaced on top of the pillow lava sheet above 700 m asl. Locally this
542 unit was erupted into subaerial conditions (Figure 6), but subaqueous deposits immediately
543 above and laterally transitional to these exposures suggest that these deposits do not represent
544 a permanent or long-standing lake level. Unit 2 lavas also experienced local post-emplacment
545 interaction with ice as evidenced by the presence of vertical pillows along flow margins
546 recording the retreat of a confining ice wall, as well as local scour and large isolated blocks of
547 lava and tuff on topographic highs that are likely glacial erratics. Additionally, the presence of
548 local diamictite (Dm 2) indicates that ice was present during and after the eruption. The
549 diamictite contains clasts of Unit 2 lava which is evidence of a local advance of the ice mass
550 leading to partial erosion of Unit 2.

551 After the emplacement of the diamictite, basaltic activity re-initiated with a more limited
552 distribution of effusive pillow lava sheets (Unit 3). This was then followed by numerous explosive
553 fissure eruptions producing a series of tindars, local subaqueous lava flows, and inter-ridge
554 depositional centers (Units 3 and 4). This was followed by Unit 5, comprising the most
555 voluminous episode of tindar formation. Near the caldera rim this unit contains heterolithic lapilli
556 tuffs that include both subaerially and subaqueously erupted clasts (Figure 6). This was followed
557 by the localized subaqueous eruption of Unit 6 porphyritic pillow mounds that drape over the
558 northeastern corner of Austurfjöll from 1160 m asl to the base of the massif (600 m asl). This
559 unit contains local examples of lava-ice interaction in the form of laterally confined radially
560 fractured lava flows. The uppermost unit of Austurfjöll is Unit 7, which is composed entirely of
561 localized subaerial lava breccias sits on the caldera rim.

562 The eruptive unit map (Figure 10) and constructional features of the massif can be used
563 to extrapolate potential cross-sections of the massif (see Online Resource 2). The
564 predominance of subaqueous textures preserved by these deposits indicates the presence of a
565 recurring ice-confined meltwater lake or lakes that were subject to drainage and refilling events
566 (Figure 11).

567 Based on observations at Austurfjöll it is likely that basaltic glaciovolcanic activity within
568 thick ice sheets (>700 m ice as constrained by the thickness of subaqueous deposits) initiated
569 with the formation of large pillow lava sheets with associated local breccias. This activity was
570 followed by the eruption of overlapping tindars as explosive activity increased as Austurfjöll built
571 up and confining pressures above newer vents were commensurately reduced. This phase
572 likely occurred in a large open ice-confined lake, if one was not already present (Figure 11).
573 The abundance of fissure-controlled geometries suggests that all eruptive units at Austurfjöll
574 may have been fissure-fed, including the pillow lava sheets. These fissure vents were widely
575 distributed over the 48 km² area now covered by the Austurfjöll massif (Figure 8). Eruptive units
576 have wide lateral distribution indicating that multiple vents were active during each eruptive
577 phase (Figure 10).

578 Austurfjöll contains deposits that predominantly record the interaction of magma with
579 water, with a notable transition from effusive pillow lava sheets to explosive tindar forming
580 activity (Table 4). The onset of explosive activity during an ice-confined eruption can be the
581 result of a change in internal eruptive conditions or external environmental conditions, or a
582 combination of the two. Internal conditions include eruptive mass discharge rate, gas content, or
583 crystal content. External conditions include an increase of infiltration of water into a vent, or
584 depressurization as a result in the elevation gain of the eruptive vent and/or a decrease in the
585 level of the confining water due to drainage. Evidence for a combination of triggering
586 mechanisms can be found in textural signatures of the primary deposits lapilli and ash tuffs (Lt1,
587 At1, Lt2, and At2). Detailed investigation of the Lt1 facies revealed that both magmatic and
588 phreatomagmatic activity contributed to the production of fragmental material at Austurfjöll. In
589 particular, an increase in mass discharge rate in an aqueous environment with a changing water
590 level triggered local transitions from effusive to explosive activity (Graettinger et al. 2013b).
591 Similarly, the common transition from regular pillowed lavas (PI1) to irregular pillowed lavas
592 (PI2) indicates that subtle variations in the eruptive flux were common during the formation of
593 pillow lava sheets that dominate Units 2 and 3.

594 At the same time, local textural variations indicate the eruptive environment was variable
595 during the construction of Austurfjöll. Large channels (100 m in diameter) cross-cut Unit 2

596 primary and remobilized lapilli tuffs, and are filled with bedded ash tuffs. Such channels indicate
597 that drainage of large volumes of water occurred while fragmental materials were
598 unconsolidated, and channels were filled by multiple pulses and / or discrete sediment gravity
599 flows (Figure 7b). Stratigraphically younger units at high elevations, such as Unit 6 (1160 m asl),
600 preserve localized subaqueous effusive-only activity. Pillow fragments in the breccias found
601 along the caldera rim (>1200 m asl) suggest ice-confined lake levels higher than the current top
602 of the massif. Additionally, small outcrops of subaerial lavas (Unit 2 and Unit 3) are found
603 interbedded and transitioning into pillowed lavas, and indicate an increase in water level during
604 the construction of the massif. This suggests that the growth of Austurfjöll as a whole was
605 influenced by a mechanism that produced a near permanent shift from effusive to explosive
606 activity, with variations in the lake level that produced local emergence and flooding. As the
607 initial effusion-dominated pillow lava sheets result in an overall increase in elevation of 100 m
608 and, therefore, a decrease in the potential water column over the eruptive vents, the simplest
609 solution for massif-wide eruption behavioral changes is for the depressurization associated with
610 the decreased water depth to enable the transition to explosive activity. This growth trend was
611 accompanied by drainage events, fluctuations in eruptive flux, and continued melting of the
612 confining ice sheet.

613 The lithofacies distribution and deposit textures enable inferences about the
614 configuration of ice and meltwater lakes during the construction of Austurfjöll. The presence of
615 vertical pillow lavas (Unit 2) and radial cooling cracks in non-pillowed lavas (Unit 6) indicate that
616 the confining ice was proximal to the growing massif. Diamictite deposits between Unit 2 and
617 Unit 3 indicate that this ice locally re-advanced onto the massif and eroded lavas between
618 eruptive units. Additionally, localized subaerial deposits, or subaerial components in clastic units
619 (i.e. Lt3) reflect variable water levels during the construction of Austurfjöll, likely related to
620 drainage and refilling of the ice-confined lake level. These features suggest that there was not a
621 single stable lake present at Austurfjöll during construction. More likely, the growth Austurfjöll
622 was associated with the formation of numerous ephemeral meltwater lakes impacted by variable
623 configurations of confining ice and eruptive activity (Figure 11). The transitions between
624 subaerial and subaqueous lithofacies at Austurfjöll are highly localized, unlike extensive
625 passage zones described tuya and tindar constructs in Iceland and British Columbia (Werner et
626 al. 1996; Skilling et al. 2009; Russell et al. 2013) and Antarctica (Smellie et al. 2013), and reflect
627 not only a variable lake level, but restricted bodies of meltwater as well as extensive massif
628 covering lakes. The extent of these lakes were likely influenced by the area of the active vent
629 over time, as there is no evidence of a long term established passage zone across the massif at

630 any elevation. Historical observations of vent proximal ice during the 1996 Gjalp eruption
631 indicated that the ice responded rapidly to the presence, and absence of ongoing eruptive
632 activity (Gudmundsson et al. 1997). The extent of the pillow lava sheets indicate that there may
633 have been a fairly large body of ice-confined meltwater early in the history of Austurfjöll, while
634 smaller eruptive units, and individual tindars, may reflect limited bodies of meltwater between
635 Austurfjöll and the confining ice mass. The thickness of the sequence and the absence of
636 significant subaerial facies reflect the thickness of ice present during the construction of the
637 massif (ca. 700-900 m), which agrees with its position near the center of the modeled
638 Weichselian ice sheet (Hubbard et al. 2006).

639

640 **Multi-vent fissure-fed glaciovolcanic massif**

641 The multi-vent construction of Austurfjöll contrasts with the morphology of more familiar
642 tuyas and tindars. Tuyas have focused or centralized vent locations as in Herðubreið (Werner et
643 al. 1996, Werner and Schmincke 1999), and Hlöðufell (Skilling 2009) in Iceland and Hoodoo
644 Mountain (Edwards et al. 2002), Mathew's Tuya (Edwards et al. 2011) and Kima' Kho (Ryane et
645 al. 2011) in British Columbia Canada. Each case is marked by distinctive lithofacies such as a
646 subaerial lava cap with lava deltas (that can define a passage zone), that reflect prolonged
647 subaerial activity (Skilling 1994, 2009; Werner and Schmincke 1999; Smellie et al. 2008; Russell
648 et al. 2013). There is no preserved evidence of prolonged subaerial activity at Austurfjöll.

649 Tindars are linear features constructed from vents aligned along an eruptive fissure, and
650 each tindar is considered to be the product of one eruptive episode, like at Helgafell (Schopka et
651 al. 2006), Sveifluhals (Mercurio 2011), and Undirhlíðar (Pollock et al. 2014) in Iceland. The
652 tindars at Austurfjöll are broadly similar to tindars described elsewhere (Mercurio 2011), with an
653 important difference at Austurfjöll being the close proximity, and overlapping, of a large number
654 of tindars. Additionally, the pillow lava sheets and the pillow mounds at Austurfjöll have not been
655 observed in similar abundance at either tuyas or tindars. Much larger pillow mounds have been
656 described in British Columbia (Canada) by Hickson (2000) as independent edifices with
657 diameters up to 2 km, in contrast to the decimeter examples at Austurfjöll. This size discrepancy
658 reflects the influence of the multi-vent, fissure-dominated construction of Austurfjöll.

659 The overall structure of Austurfjöll has little in common with tuyas but much in common
660 with tindars, reflecting a new mechanism for glaciovolcanic massif construction via multiple
661 tindars as a part of a long-lived central volcano. The westernmost sector of the Austurfjöll
662 glaciovolcanic massif has been removed by two caldera collapses, one in 1875 AD, and an
663 earlier collapse of unknown age. Additional glaciovolcanic massifs at Askja are present in the

664 North East and Thorvaldstindur along the southern margin of the current lake. The overall
665 complex presents a unique morphology that has yet to be considered in planetary searches for
666 glaciovolcanic constructs (e.g. Ghatan and Head 2002; Houvis et al. 2008; Martinez-Alonso et
667 al. 2011).

668 The architecture of Austurfjöll indicates that it was constructed via multiple glaciovolcanic
669 eruptions of modest volume. The Weichselian activity has a strong parallel in Holocene
670 volcanism at Askja, where similar activity (i.e. fissure eruptions of modest volume) has persisted
671 from the early Holocene to the present day (Annertz 1985; Höskuldsson 1987; Sigvaldason et
672 al. 1992; Kuritani et al. 2011; Hartley et al. 2016) the most recent eruption being in 1961
673 (Thorarinsson and Sigvaldason 1962). It is likely that other large basaltic volcanoes in Iceland
674 that interacted with an ice sheet also preserve evidence of prolonged multi-vent, multi-fissure
675 eruptions through multiple ice-confined lakes.

676

677 **Conclusions**

678 The glaciovolcanic history of Austurfjöll represents the construction of a complicated
679 fissure-fed massif dominated by pillow lava sheets and numerous (>40) overlapping tindars in
680 several ice-confined lakes, during the last (Weichselian) glacial period. This study represents
681 the first description of a disperse multi-vent glaciovolcanic massif forming part of long-lived
682 basaltic volcano in Iceland. The glaciovolcanic activity of Austurfjöll contributed a significant
683 volume of basaltic material to Askja volcano through the formation of pillow lava sheets and
684 overlapping tindars with seven recognizable eruptive units. The lithofacies indicate that activity
685 shifted from predominantly effusive activity of early constructional phases to explosive-
686 dominated phases as the massif increased in elevation, and was subject to temporary meltwater
687 drainage events with local increases in eruptive flux. Austurfjöll expands our understanding of
688 the longevity and chemical variability at Icelandic basaltic volcanoes, and the effects on ice
689 sheets present at the time of eruption. In particular, Austurfjöll represents the first example of a
690 complicated and widely dispersed vent system that resulted in a newly described morphology
691 and constructional history relative to previously described glaciovolcanic systems in Iceland,
692 and around the world. This broader distribution of vents, in contrast to more centralized tuyas
693 has important implications for the influence of a long-lived basaltic volcano on the overlying ice
694 sheet and the generation of multiple variable meltwater lakes. This new glaciovolcanic geometry
695 should be considered in the future identification of glaciovolcanic massifs on Earth and Mars.
696 However, if the structure is realized to be unique to Askja, it raises important questions about

697 the tectonic setting of central Iceland and the influence of the hotspot, or perhaps the role of
698 other eruptions, including caldera forming events, on the structure of Askja volcano.

699

700 **Acknowledgments**

701 This work was made possible by a National Science Foundation grant to IPS, DMcG, and AH
702 (Award number 0910526). Our gratitude goes to Haskolí Islands, NORVOLK, and the
703 Vatnajökull National Park, for field logistics and permits. Field assistance from Robin Wham,
704 Rachel Lee, Antonia Lema, Kevin Reath, and Mary Kate Ellis was invaluable. Comments by K.
705 Russell, an anonymous reviewer, and the editors greatly improved the manuscript.

706

707 **References**

- 708 Annertz K, Nilsson M, Sigvaldason GE (1985) The postglacial history of Dyngjufjöll In:
709 NORVULK. Nordic Volcanological Institute, Reykjavik p22
- 710 Baer G (1995) Fracture propagation and magma flow in segmented dykes: Field evidence and
711 fabric analyses, Makhtesh Ramon, Israel. In: Baer G, Heimann A (eds) Physics and Chemistry
712 of Dykes. Geological Survey of Israel, Balkema pp 125-140
- 713 Bennett MR, Huddart D, Waller RI (2006) Diamict fans in subglacial water-filled cavities- a new
714 glacial environment. Quaternary Science Reviews 25:3050-3069,
715 doi:10.1016/j.quascirev.2006.05.004
- 716 Bergh SG, Sigvaldason GE (1991) Pleistocene mass-flow deposits of basaltic hyaloclastite on a
717 shallow submarine shelf, South Iceland. Bulletin of Volcanology 53:597-611
- 718 Carey R, Houghton BF, Thordarson T (2009) Abrupt shifts between wet and dry phases of the
719 1875 eruption of Askja Volcano: Microscopic evidence for macroscopic dynamics. Journal of
720 Volcanology and Geothermal Research 184:256-270. doi: 10.1016/j.jvolgeores.2009.04.003
- 721 Carlisle D, (1963) Pillow breccias and their aquagene tuffs, Quadra Island, British Columbia.
722 The Journal of Geology 71: 48-71.
- 723 Carrivick JL, Russell AJ, Rushmer EL, Tweed FS, Marren PM, Deeming H, Lowe OJ (2009)
724 Geomorphological evidence towards a de-glacial control on volcanism. Earth Surface
725 Processes and Landforms 34:1164-1178, doi:10.1002/esp.1811
- 726 Dimroth E, Pierre C, Leduc M, Sanshagrín Y (1978) Structure and organization of Archean
727 subaqueous basalt flows, Rouyn-Noranda area, Quebec, Canada. Canadian Journal of Earth
728 Science 15:902-918

729 Doyle MG (2000) Clast shape and textural associations in peperite as a guide to hydromagmatic
730 interactions: Upper Permian basaltic and basaltic andesite examples from Kiama, Australia.
731 Australian Journal of Earth Sciences 47:167-177, doi:10.1046/j.1440-0952.2000.00773.x

732 Edwards BR, Russell JK, Anderson RG (2002) Subglacial, phonolitic volcanism at Hoodoo
733 Mountain volcano, northern Canadian Cordillera. Bulletin of Volcanology 64:254-272,
734 doi:10.1007/s00445-002-0202-9

735 Edwards BR, Skilling IP, Cameron B, Haynes C, Lloyd A, Hungerford JHD (2009) Evolution of
736 an englacial volcanic ridge: Pillow Ridge tindar, Mount Edziza volcanic complex, NCVP, British
737 Columbia, Canada. Journal of Volcanology and Geothermal Research 185:251-275,
738 doi:10.1016/j.jvolgeores.2008.11.015

739 Edwards BR, Russell JK, Simpson K (2011) Volcanology and petrology of Mathews Tuya,
740 northern British Columbia, Canada: glaciovolcanic constraints on interpretations of the 0.730 Ma
741 Cordilleran paleoclimate. Bulletin of Volcanology 73:479-496, doi:10.1007/s00445-010-0418-z

742 Edwards BR, Gudmundsson MT, Russell JK (2015) Glaciovolcanism. In: Sigurdsson H (eds)
743 The Encyclopedia of Volcanoes, 2nd Edition. Academic Press, pp 377-393, doi:10.1016/B978-
744 0-12-385938-9.00020-1

745 Einarsson P (2008) Plate boundaries, rifts and transforms in Iceland. Jokull 58: 35-58.

746 Ghatan G, Head JW (2002) Candidate subglacial volcanoes in the south polar region of Mars:
747 Morphology, morphometry, and eruption conditions 107: 2-1-1-19. doi: 10.1029/2001JE001519

748 Goto Y, McPhie J (2004) Morphology and propagation styles of Miocene submarine basanite
749 lavas at Stanley, northwestern Tasmania, Australia. Journal of Volcanology and Geothermal
750 Research 130:307-328, doi:10.1016/S0377-0273(03)00311-1

751 Graettinger AH, Skilling IP, McGarvie DW, Höskuldsson A (2012) Intrusion of basalt into frozen
752 sediments and generation of Coherent-Margined Volcaniclastic Dikes (CMVDs). Journal of
753 Volcanology and Geothermal Research 217-218:30-38, doi:10.1016/j.jvolgeores.2011.12.008

754 Graettinger AH, Ellis MK, Skilling IP, Reath K, Ramsey MS, Lee RJ, Hughes CG, McGarvie DW
755 (2013a) Remote sensing and geologic mapping of glaciovolcanic deposits in the region
756 surrounding Askja (Dyngjufjöll) volcano, Iceland. International Journal of Remote Sensing
757 34:7178-7198, doi:10.1080/01431161.2013.817716

758 Graettinger AH, Skilling IP, McGarvie DW, Höskuldsson A (2013b) Subaqueous basaltic
759 magmatic explosions trigger phreatomagmatism: a case study from Askja, Iceland. Journal of
760 Volcanology and Geothermal Research 264:17-35, doi:10.1016/j.jvolgeores.2013.08.001

761 Gregg TKP, Fink JH (1995) Quantification of submarine lava-flow morphology through analog
762 experiments. Geology 23:73-76

- 763 Gregg TKP, Smith D (2003) Volcanic investigations of the Puna Ridge, Hawai'i: relations of lava
764 flow morphologies and underlying slopes. *Journal of Volcanology and Geothermal Research*
765 126:63-77, doi:10.1016/S0377-0273(03)00116-1
- 766 Gudmundsson MT, Sigmundsson F, Björnsson H (1997) Ice-volcano interaction of the 1996
767 Gjalp subglacial eruption, Vatnajökull, Iceland. *Nature* 389:954-957
- 768 Hartley ME, Thordarsson T, de Joux A (2016) Postglacial eruptive history of the Askja region,
769 North Iceland. *Bulletin of Volcanology* 78:28 doi: 10.1007/s00445-016-1022-7
- 770 Hickson CJ (2000) Physical controls and resulting morphological forms of Quaternary ice-
771 contact volcanoes in western Canada. *Geomorphology* 32:239-261
- 772 Höskuldsson Á (1987) Some chemical properties of the Askja volcanic center In: Nordic
773 Volcanological Institute, University of Iceland Reykjavík
- 774 Höskuldsson Á, Sparks RSJ, Carrol MR (2006) Constraints on the dynamics of subglacial basalt
775 eruptions from geological and geochemical observations at Kverkfjöll, NE-Iceland. *Bulletin of*
776 *Volcanology* 68:689-701, doi:10.1007/s00445-005-0043-4
- 777 Hungerford JDG, Edwards BR, Skilling IP, Cameron BI (2014) Evolution of a subglacial basaltic
778 lava flow field: Tennena volcanic center, Mount Edziza volcanic complex, British Columbia,
779 Canada. *Journal of Volcanology and Geothermal Research* 272:39-58,
780 doi:10.1016/j.jvolgeores.2013.09.012
- 781 Houvis N, Lea-Cox A, Turowski JM (2008) Recent volcano-ice interaction and outburst flooding
782 in a Mars polar cap re-entrant. *Icarus* 197:23-38. doi: 10.1016/j.icarus.2008.04.020
- 783 Jakobsson SP, Gudmundsson MT (2008) Subglacial and intraglacial volcanic formations in
784 Iceland. *Jökull* 58:179-196
- 785 Jonasson K (1994) Rhyolite volcanism in the Krafla central volcano, north-east Iceland. *Bulletin*
786 *of Volcanology* 56: 516-528.
- 787 Kennish MJ, Lutz RL (1998) Morphology and distribution of lava flows on mid-ocean ridges: a
788 review. *Earth-Science Reviews* 43:63-90, doi:10.1016/j.geomorph.2006.12.002
- 789 Komatsu G, Arzhannikov SG, Arzhannikova AV, Ershov K (2007) Geomorphology of subglacial
790 volcanoes in the Azas Plateau, the Tuva Republic Russia. *Geomorphology* 88:312-328
- 791 Kralj P (2012) Facies architecture of the Upper Oligocene submarine Smrekovec stratovolcano,
792 Northern Slovenia. *Journal of Volcanology and Geothermal Research* 247-248:122-138,
793 doi:10.1016/j.jvolgeores.2012.07.016
- 794 Kuritani T, Yokoyama T, Kitagawa H, Kobayashi K, Nakamura E (2011) Geochemical evolution
795 of historical lavas from Askja Volcano, Iceland: Implications for mechanisms and timescales of
796 magmatic differentiation. *Geochemica et Cosmochimica Acta* 75:570-587,
797 doi:10.1016/j.gca.2010.10.009

798 Lacasse C, Sigurdsson H, Carey SN, Johannesson H, Thomas LE, Rogers NW (2007) Bimodal
799 volcanism at the Katla subglacial caldera, Iceland: insight into the geochemistry and
800 petrogenesis of rhyolitic magmas. *Bulletin of Volcanology* 69:373. doi: 10.1007/s00445-006-
801 0082-5

802 Loughlin SC (2002) Facies analysis of proximal subglacial and proglacial volcanoclastic
803 successions at the Eyjafjallajökull. In: Smellie JL, Chapman MG (ed) *Volcano-Ice Interaction on*
804 *Earth and Mars*. The Geological Society of London, London, pp 149-178

805 Macdonald R, Sparks R, Sigurdsson H, Matthey D, McGarvie D, Smith R (1987) The 1875
806 eruption of Askja volcano, Iceland: Combined fractional crystallization and selective
807 contamination in the generation of rhyolitic magma. *Mineralogical Magazine* 51: 183-202.
808 doi:10.1180/minmag.1987.051.360.01

809 Maicher D, White JDL, Batiza R (2000) Sheet hyaloclastite: density-current deposits of quench
810 and bubble-burst fragments from thin, glassy sheet lava flows, Seamount Six, Eastern Pacific
811 Ocean. *Marine Geology* 171:75-94, doi:10.1016/S0025-3227(00)00109-2

812 Martinez-Alonso S, Mellon MT, Banks MA, Keszthelyi LP, McEwen AS, The HiRISE Team
813 (2011) Evidence of volcanic and glacial activity in Chryse and Acidalia Planitiae, Mars. *Icarus*
814 212: 597-621. doi: 10.1016/j.icarus.2011.01.004

815 McPhie J, Doyle MG, Allen CC (1993) *Volcanic Textures: A guide to the interpretation of*
816 *textures in volcanic rocks*. CODES Key Centre, University of Tasmania Hobart p. 198

817 Mercurio E (2011) Processes, products and depositional environments of ice-confined basaltic
818 fissure eruptions: a case study of the Sveifluhals volcanic complex, SW Iceland. Unpublished
819 dissertation. Department of Geology and Planetary Science, University of Pittsburgh

820 Parfitt EA, Gregg TKP, Smith D (2002) A comparison between subaerial and submarine
821 eruptions at Kilauea Volcano, Hawaii: implications for the thermal viability of lateral feeder dikes.
822 *Journal of Volcanology and Geothermal Research* 113:213-242, doi:10.1016/S0377-
823 0273(01)00259-1

824 Pollock M, Edwards BR, Hauksdottir S, Alcorn R, Bowman L (2014) Geochemical and
825 lithostratigraphic constrains on the formation of pillow-dominated tindars from Undirhlíðar
826 quarry, Reykjanes Peninsula, southwest Iceland. *Lithos* 200-201:314-333,
827 doi:10.1016/j.lithos.2014.04.023

828 Ryane C, Edwards BR, Russell JK (2011) The volcanic stratigraphy of Kima'Kho Mountain: A
829 Pleistocene tuya, northwestern British Columbia. In: *Geological Survey of Canada Current*
830 *Research*. Geological Survey of Canada, doi:10.4095/289196

831 Rivalta E, Dahm T (2006) Acceleration of buoyancy-driven fractures and magmatic dikes
832 beneath the free surface. *Geophysical Journal International* 166:1424-1439, doi:10.1111/j.1365-
833 246X.2006.02962.x

- 834 Russell JK, Edwards BR, Porritt LA (2013) Pyroclastic passage zones in glaciovolcanic
835 sequences. *Nature* 4 doi:10.1038/ncomms2829
- 836 Russell JK, Edwards BR, Porritt LA, Ryane C (2014) Tuya: a descriptive genetic classification.
837 *Quaternary Science Reviews* 87:70-81, doi:10.1016/j.quascirev.2014.01.001
- 838 Sansone FJ, Smith JR (2006) Rapid mass wasting following nearshore submarine volcanism on
839 Kilauea volcano, Hawaii. *Journal of Volcanology and Geothermal Research* 151:133-139,
840 doi:10.1016/j.jvolgeores.2005.07.026
- 841 Schopka HH, Gudmundsson MT, Tuffen H (2006) The formation of Helgafell, southwest Iceland,
842 a monogenetic subglacial hyaloclastite ridge: Sedimentology, hydrology and volcano-ice
843 interaction. *Journal of Volcanology and Geothermal Research* 152:359-377,
844 doi:10.1016/j.jvolgeores.2005.11.010
- 845 Sigvaldason GE (1968) Structure and products of subaquatic volcanoes in Iceland.
846 *Contributions to Mineralogy and Petrology* 18:1-16
- 847 Sigvaldason GE, Annertz K, Nilsson M (1992) Effect of glacier loading/deloading on volcanism:
848 postglacial volcanic production rate of the Dyngjufjöll. *Bulletin of Volcanology* 54:385-392
- 849 Skilling IP (1994) Evolution of an englacial volcano: Brown Bluff, Antarctica. *Bulletin of*
850 *Volcanology* 56:573-591
- 851 Skilling IP (2009) Subglacial to emergent basaltic volcanism at Hlöðufell, south-west Iceland: A
852 history of ice-confinement. *Journal of Volcanology and Geothermal Research* 185:276-289,
853 doi:10.1016/j.jvolgeores.2009.05.023
- 854 Skilling IP, White JDL, McPhie J (2002) Peperite: a review of magma-sediment mingling.
855 *Journal of Volcanology and Geothermal Research* 114:1-17, doi:10.1016/S0377-
856 0273(01)00278-5
- 857 Smellie JL (2006) The relative importance of supraglacial versus subglacial meltwater escape in
858 basaltic subglacial tuya eruptions: An important unresolved conundrum. *Earth-Science Review*
859 74:241-268 doi:10.1016/j.earscirev.2005.09.004
- 860 Smellie JL, Johnson JS, McIntosh WC, Esser R, Gudmundsson MT, Hambrey MJ, van Wyk de
861 Vries B (2008) Six million years of glacial history recorded in volcanic lithofacies of the James
862 Ross Island Volcanic Group, Antarctic Peninsula. *Palaeogeography, Palaeoclimatology,*
863 *Palaeoecology* 260:122-148. doi:10.1016/j.palaeo.2007.08.011
- 864 Smellie JL (2008) Basaltic subglacial sheet-like sequences: Evidence for two types with different
865 implications for the inferred thickness of associated ice. *Earth-Science Reviews* 88:60-88,
866 doi:10.1016/j.earscirev.2008.01.004
- 867 Smellie JL, Hole MJ (1997) Products and processes in Pliocene-Recent, subaqueous to
868 emergent volcanism in the Antarctic Peninsula: examples of englacial Surtseyan volcano
869 construction. *Bulletin of Volcanology* 58:628-646

870 Stevenson JA, Smellie JL, McGarvie DW, Gilbert JS, Cameron BI (2009) Subglacial
871 intermediate volcanism at Kerlingarfjöll, Iceland: magma-water interactions beneath thick ice.
872 Journal of Volcanology and Geothermal Research 185: 337-351,
873 doi:10.1016/j.volgeores.2008.12.016

874 Strand K (1987) Models for the deposition and the role of external water in explosive volcanism
875 of the Dyngjufjöll Late Pleistocene-Holocene central volcano complex in North Iceland. In:
876 Nordic Volcanological Institute, University of Iceland Reykjavik

877 Stroncik N, Schmincke H-U (2002) Palagonite- a review. International Journal of Earth Science
878 (Geol Rundsch) 91:680-697, DOI 10.1007/s00531-001-0238-7

879 Thorarinsson S, Sigvaldason G (1962) The eruption in Askja, 1961 a preliminary report.
880 American Journal of Science 260:641-651

881 Tucker DS, Scott KM (2009) Structures and facies associated with the flow of subaerial basaltic
882 lava into a deep freshwater lake: the Sulphur Creek lava flow, North Cascades, Washington.
883 Journal of Volcanology and Geothermal Research 185:311-322,
884 doi:10.1016/j.volgeores.2008.11.028

885 Vezzoli LM, Hauser N, Omarini R, Mazzuoli R, Acocella V (2008) Non-explosive magma-water
886 interaction in a continental setting: Miocene examples from the Eastern Cordillera. Bulletin of
887 Volcanology 71:509, doi: 10.1007/s00445-008-0239-5

888 Walker GPL (1992) Morphometric study of pillow-size spectrum among pillow lavas. Bulletin of
889 Volcanology 54:459-474

890 Watton TJ, Jerram DA, Thordarson T, Davies RJ (2013) Three-dimensional lithofacies
891 variations in hyaloclastite deposits Journal of Volcanology and Geothermal Research 250:19-
892 33, doi:10.1016/j.volgeores.2012.10.011

893 Werner R, Schmincke H-U, Sigvaldason GE (1996) A new model for the evolution of table
894 mountains: volcanological and petrological evidence from Herdubreid and Herdubreidartögl
895 volcanoes (Iceland) Geol Rundsch 85:390-397

896 Werner R, Schmincke H-U (1999) Englacial vs lacustrine origin of volcanic table mountains:
897 evidence from Iceland. Bulletin of Volcanology 60:335-354

898 White JDL (1996) Pre-emergent construction of a lacustrine basaltic volcano, Pahvant Butte,
899 Utah (USA). Bulletin of Volcanology 58:249-262

900 White JDL (2000) Subaqueous eruption-fed density currents and their deposits. Precambrian
901 Research 101:87-109, doi:10.1016/S0301-9268(99)00096-0

902 White JDL, McPhie J, Skilling IP (2000) Peperite: a useful genetic term. Bulletin of Volcanology
903 62:65-66

904 Wood DA (1976) Spatial and temporal variation in the trace element geochemistry of the
905 eastern Iceland flood basalt succession. *Journal of Geophysical Research* 81(23):4353-4360

906 Wood DA (1978) Major and Trace Element Variations in the Tertiary Lavas of Eastern Iceland
907 and their Significance with respect to the Iceland Geochemical Anomaly. *Journal of Petrology*
908 19(3):393-436

909

910

911 **Figure Captions**

912 **Fig. 1** A) Map of Iceland and study area, Askja. Major volcanic zones in Iceland are highlighted,
913 with inset of Askja volcano and Austurfjöll massif. Yellow dots indicate logs from this study,
914 black triangles are logs collected by K. Strand and A. Höskuldsson in 1980 for NORVOLK
915 (Strand 1987). B) Lithofacies map of Austurfjöll (outlined in black). Other regions studied using
916 reconnaissance survey with aerial photo support. A rhyolite dome was observed in the field but
917 not studied in detail.

918 **Fig. 2** Example images of breccia and diamictite deposits from Austurfjöll glaciovolcanic massif.
919 A) Pillow breccia (B1), where pillow forms are preserved (yellow circle around a 20 cm diameter
920 pillow fragment), B) Angular block breccia (B2) with person for scale, C) Diamictite (Dia1)
921 containing large striated rounded glacial clasts in a fine matrix units on scale are 10 cm, D)
922 Glacial outwash (Dia2) sandy diamictite containing small rounded pebbles, arrow in scale is 10
923 cm.

924 **Fig. 3** Examples of lapilli tuff deposits: A) Angular lapilli tuff (Lt1) contains glassy angular clasts
925 that may have convolute vesicles and fluidal clast shapes (yellow line around example of fluidal
926 clast), 1 cm increments on scale bar, B) Subrounded lapilli tuff (Lt2) contains isolated outsized
927 clasts in a matrix of subrounded lapilli, small divisions on scale are 1 cm, C) Red scoria lapilli
928 tuff (Lt3), dominated by subaerial components such as scoria and armored lapilli (arrows
929 indicate armored lapilli), D) lapilli heterolithic lapilli tuff (Lt4) containing diverse subrounded
930 clasts of subaqueous and subaerial components (arrows indicate different clast types R=
931 oxidized subaerial lava, D= dense basalt, Bx = porphyritic basalt).

932 **Fig. 4** Examples of ash-dominated tuff A) massive ash tuff (At1) is poorly sorted coarse ash with
933 occasional outsized clasts (blocks). Bedded lapilli tuff (At2) contains well sorted layers of coarse
934 to fine ash (B, D) displayed bedding on the centimeter to decimeter scale with rare loading
935 structures (B yellow arrows indicate loading structures, 10 cm increments on scale bar). C)
936 Alternating bedded ash tuff (At3) displays variations in bedding and grain size on the decimeters
937 with occasional sedimentary structures such as cross-bedding, or ripples.

938 **Fig. 5** Deformed domains of ash tuff (At4) are common around the massif overlying fragmental
939 deposits from breccias to tuffs. The domains contain internal sedimentary structures with
940 individual beds displaying variable sorting. The domains display dramatic folding and centimeter
941 scale convolutions. The domains have dips along fold axes as high as 85 degrees. Yellow lines
942 follow example bedding planes to highlight the intense folding. Scale bar has 10 cm increments.

943 **Fig. 6** Example stratigraphic logs from Austurfjöll. Section locations are indicated in Figure 1.
944 Lithofacies in these sections represent common associations between facies types, but cannot
945 be traced across the massif as the structure is divided by smaller constructional features (see
946 Supplementary material). Assignment to eruptive units is described in Geochemistry section.

947 **Fig. 7** Examples of major features at Austurfjöll massif. A) Isolated tindars with visible intrusive
948 core, view to southeast towards Vatnajökull. B) Eroded channel ~ 100 m wide in Astronaut Gully

949 looking towards Herðubreið. C) Pillow lava sheets (60-100 m thick) are composed of pillow
950 lavas (P11, P12) and associated breccias (B1-B2) exposed in steep sided gully on eastern edge
951 of Austurfjöll. As shown here pillow lava sheets can be composed of multiple units that fill and
952 level the topography. D) Pillow mounds occur in isolation up to 30 m high, and in clusters 15 m
953 high, overlapping other glaciovolcanic deposits, yellow line indicates tops of clustered pillow
954 mounds.

955 **Fig. 8** Hillshade produced from a 10 m DEM of Austurfjöll Askja used to indicate location of
956 vents (predominantly tindars) identified either through field relationships, topography or
957 speculation (incomplete field or topographic evidence). The distribution of the more than 50
958 surficially exposed vents results in a unique morphology of the massif and neighboring
959 Thorvaldstindur along the southern end of Öskjuvatn.

960 **Fig. 9** Variation diagrams of Austurfjöll major and trace element geochemistry. Units were
961 initially divided based on stratigraphic relationships, then samples not well constrained by
962 stratigraphy were assigned to a Unit based on trace element geochemistry characteristics of
963 recognized units. A) Total alkali versus silica plot. B) CaO vs. TiO. C- D) Incompatible trace
964 elements Nb vs Y and Zr vs Rb respectively. Incompatible element enrichment trend is: Unit 6 <
965 Unit 5 < Unit 4 < Unit 1 < Unit 2 < Unit 3 < Unit 7.

966 **Fig. 10** A) Map of eruptive units at Austurfjöll defined by stratigraphy supplemented with
967 geochemical data. B) Insert region of map to highlight the small exposure of Unit 4. C)
968 Simplified stratigraphic column of the history of the glaciovolcanic massif. Relative width of the
969 column is reflective of unit distribution, while thickness corresponds to unit thickness. The
970 appearance of macro-porphyrific units is noted. The Units that are cut by caldera faults are
971 indicated. See Online Resource 2 for cross-sections.

972 **Fig. 11** Simplified chronology of relative ice and meltwater positions based on lithofacies
973 mapping and eruptive chronology for Austurfjöll massif using an W-E section. This schematic
974 highlights the variability and recurring nature of meltwater lakes over the massif. The water and
975 ice positions given here are minimums, values in italics are maximum elevations of subaqueous
976 deposits for a given unit. Distributions and geometries that involve thicker ice or additional
977 bodies of meltwater are possible. Additional drainage events (as depicted for Unit 2) are also
978 possible. The meltwater is depicted as an open lake due to the large areal extent of the eruptive
979 deposits (Unit 2 & 3). Question marks indicate poorly constrained ice conditions.

980 **Online Resource 1** Complete geochemistry dataset of Askja samples.

981 **Online Resource 2** Example cross-sections through the Austurfjöll massif indicating the
982 development of massif as a sequence of fissure fed pillow lava sheets followed by more
983 explosive tindars. A rhyolite dome was observed but poorly constrained.

984

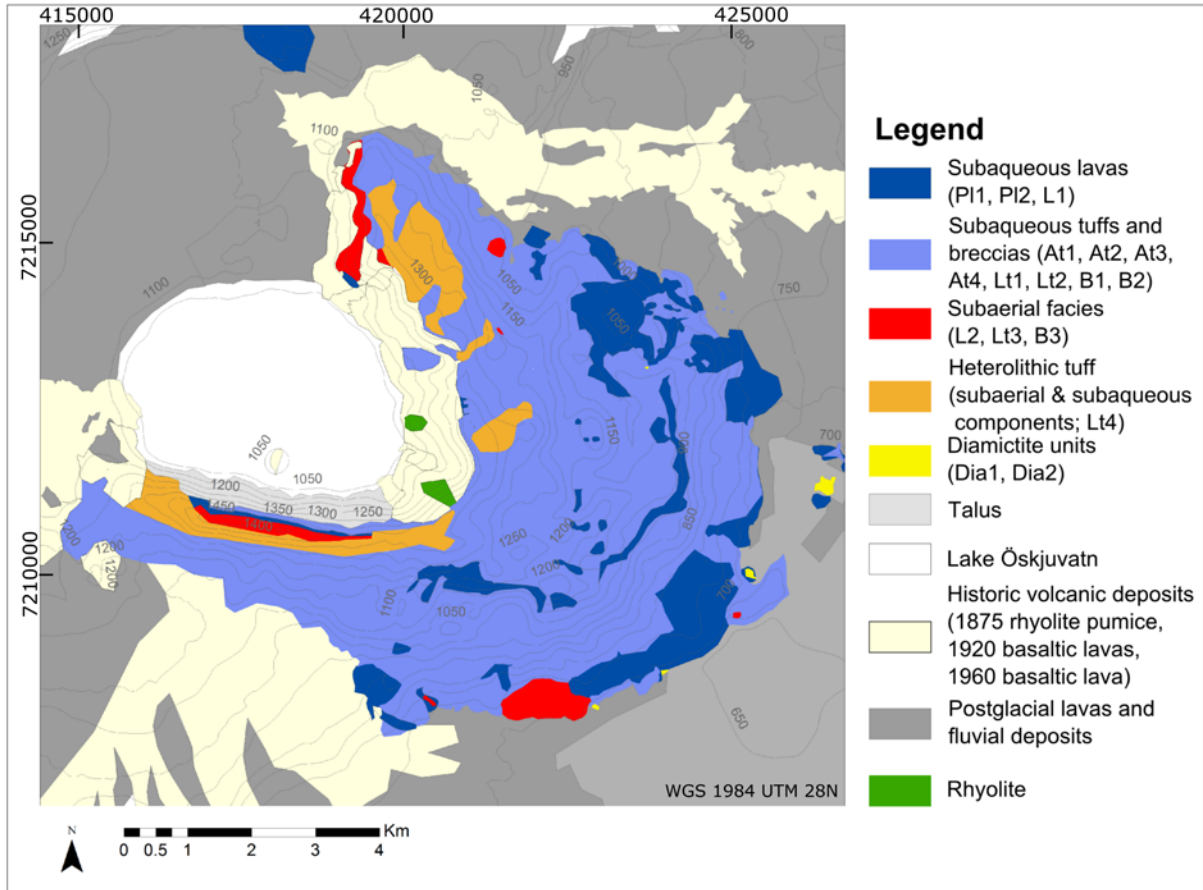
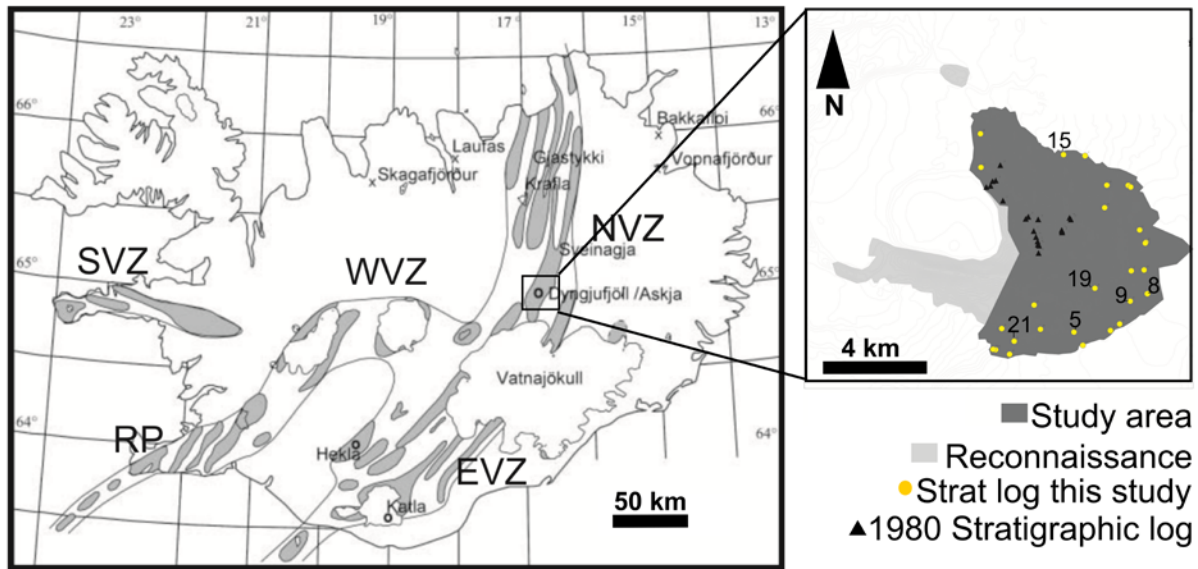


Figure 1: A) Map of Iceland and study area, Askja Iceland. Major volcanic zones in Iceland are highlighted, with inset of Askja volcano and Austurfjöll massif. Yellow dots indicate logs from this study, black triangles are logs collected by K. Strand and A. Höskuldsson in 1980 for NORVOLK (Strand 1987). Numbers for logs presented here. Light grey regions studied in less detail. B)

Simplified lithofacies map of Austurfjöll. For more detail see Graettinger et al. (2013b). Contour intervals of 50 m.

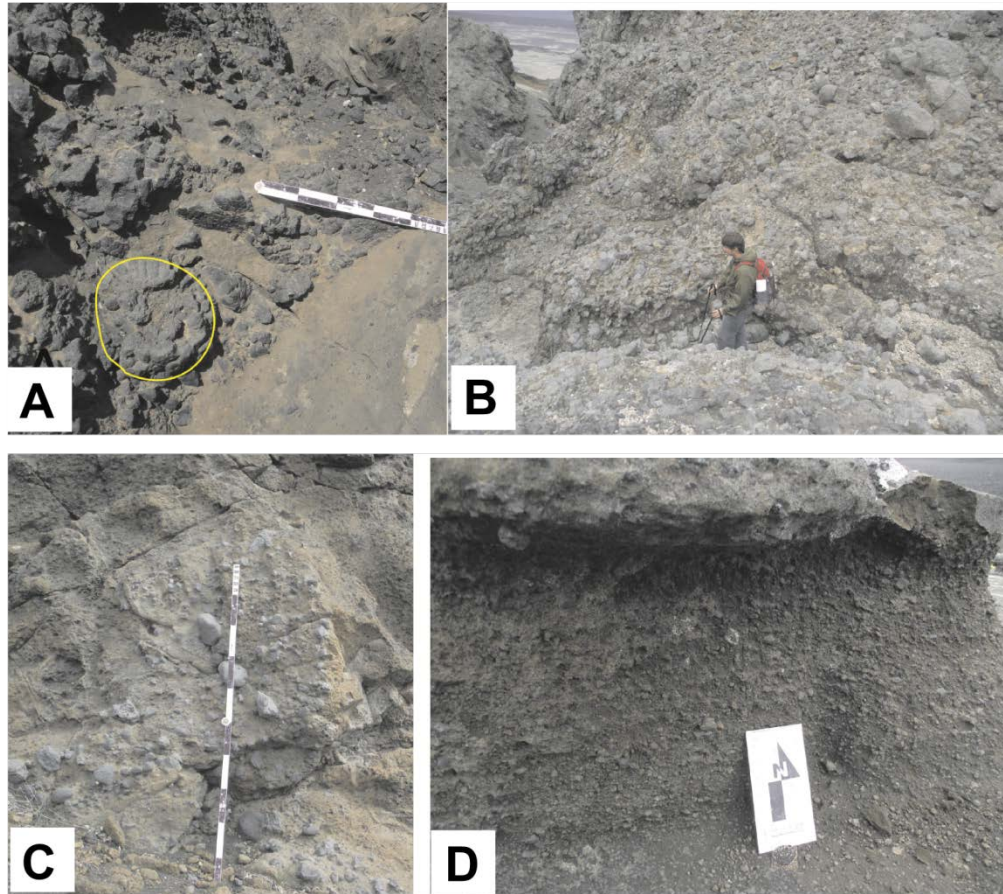


Figure 2: Example images of breccia and conglomerate deposits from Austurfjöll glaciovolcanic massif. A) Pillow breccia (B1), where pillow forms are preserved; B) Angular block breccia (B2); C) Diamicrite (Dia1) containing large striated rounded glacial clasts in a fine matrix; D) Glacial outwash (Dia2) sandy conglomerate containing small rounded pebbles.

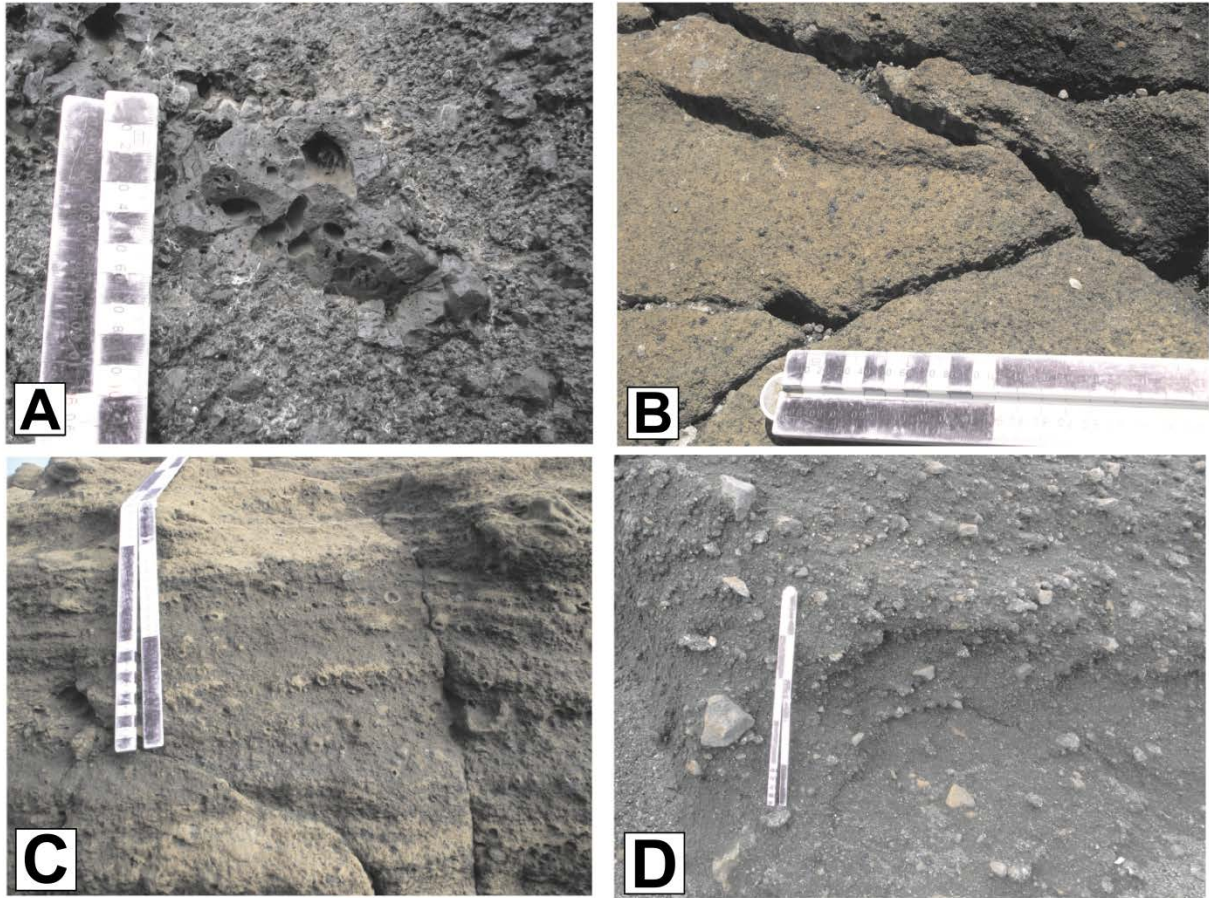


Figure 3: Examples of lapilli tuff deposits: A) Angular lapilli tuff (Lt1) contains glassy angular clasts that may have convolute vesicles and fluidal clast shapes, B) Subrounded lapilli tuff (Lt2) contains isolated outsized clasts in a matrix of subrounded lapilli, C) Red scoria lapilli tuff (Lt3), dominated by subaerial components such as scoria and armored lapilli as pictured, D) lapilli heterolithic lapilli tuff (Lt4) containing diverse subrounded clasts of subaqueous and subaerial components.

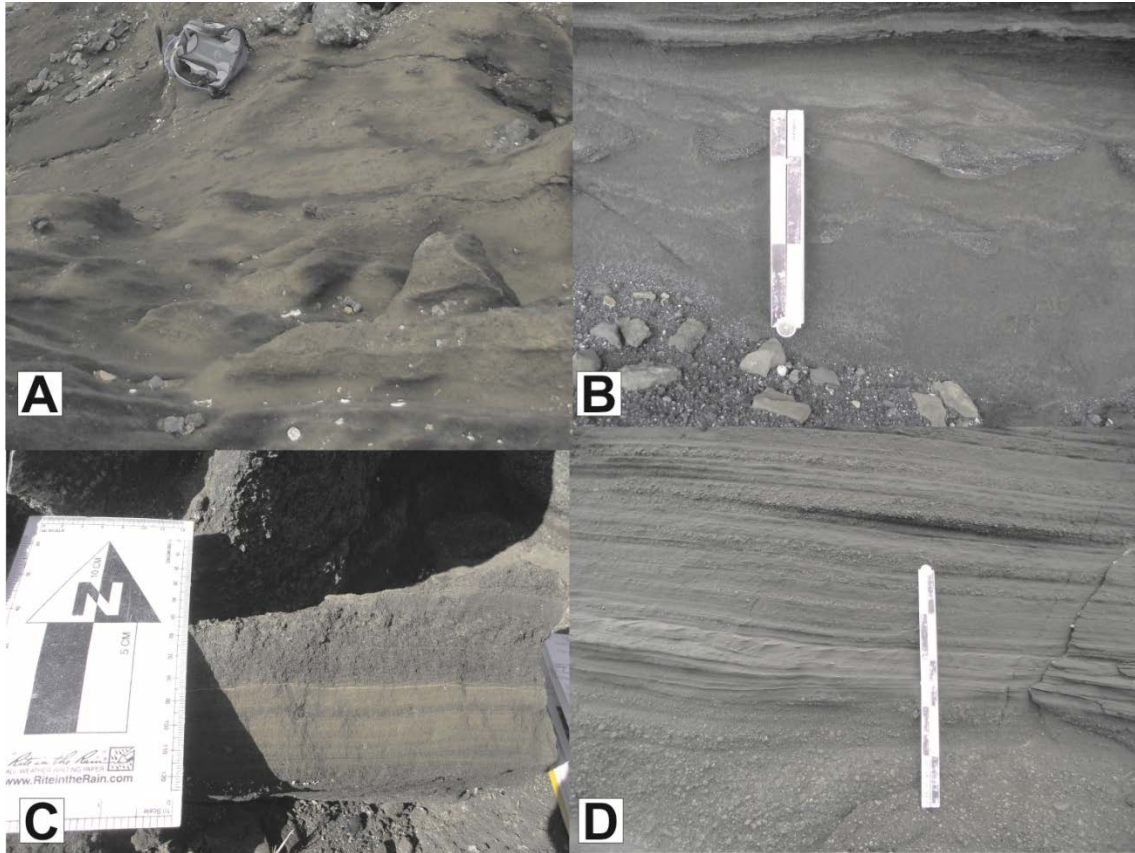


Figure 4: A) massive ash tuff (At1) is poorly sorted coarse ash with occasional outsized clasts (blocks). Bedded ash and lapilli tuff (At2) contains well sorted layers of coarse to fine ash (B, D) displayed bedding on the centimeter to decimeter scale with rare loading structures (B). C) Alternating bedded ash tuff (At3) displays variations in bedding and grain size on the decimeters with occasional sedimentary structures such as cross-bedding, or ripples.

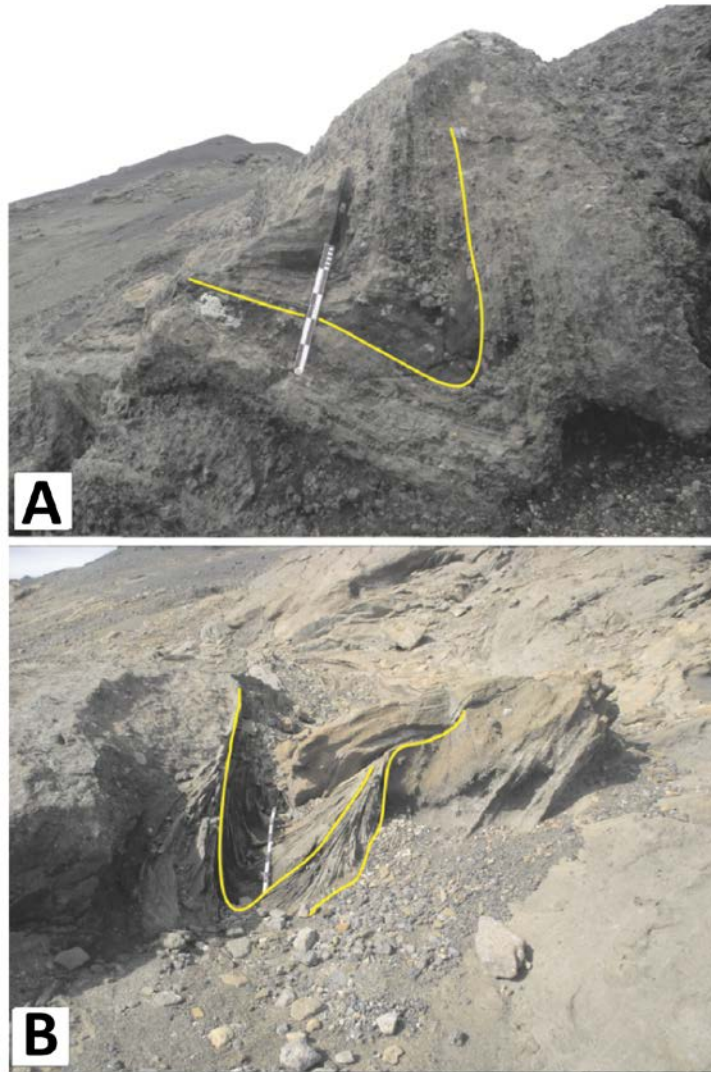


Figure 5: Deformed domains of ash tuff (At4) are common around the massif overlying fragmental units from breccias to tuffs. The domains contain internal sedimentary structures with individual beds displaying variable sorting. The domains display dramatic folding and centimeter scale convolutions. The domains have dips along fold axes as high as 85 degrees.

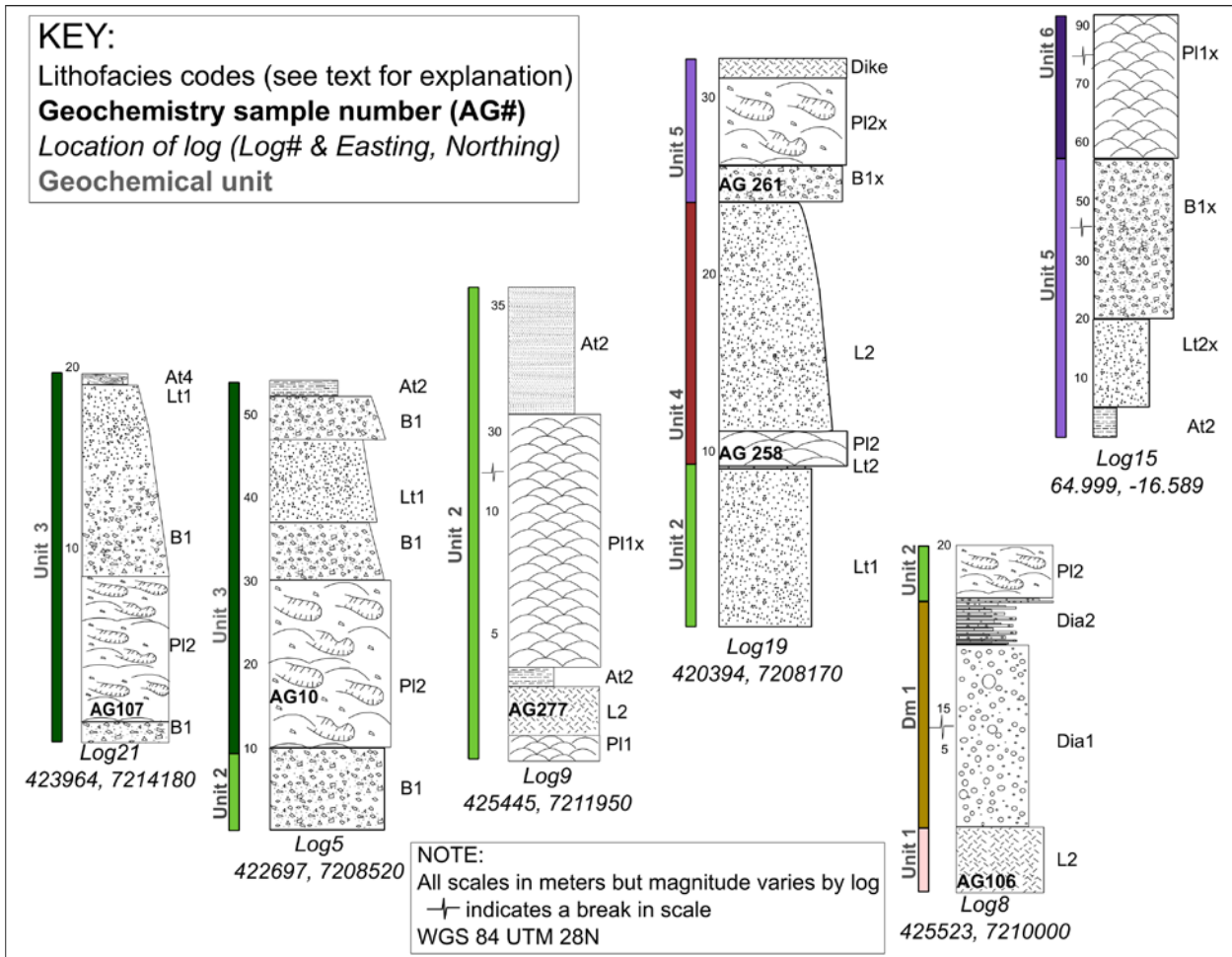


Figure 6 Example stratigraphic logs from Austurfjöll. Section locations are indicated in Figure 1. Lithofacies in these sections represent common associations between facies types, but cannot be traced across the massif as the structure is divided by smaller constructional features (see Supplementary material). Assignment to eruptive units is described in Geochemistry section.

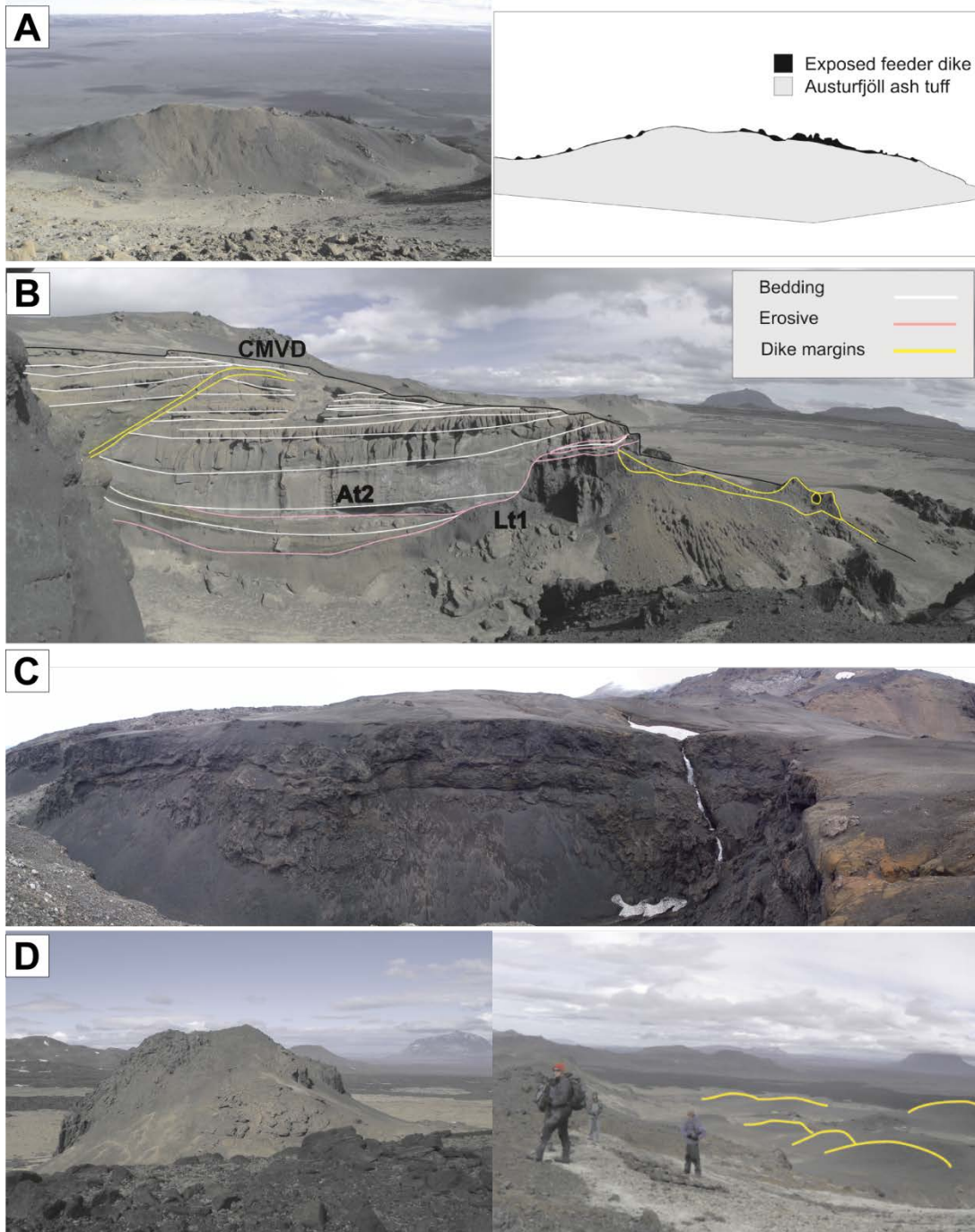


Figure 7: Examples of major features at Austurfjöll massif. A) Isolated tindars with visible intrusive core, view to southeast towards Vatnajökull. B) Eroded channel ~ 100 m wide in Astronaut Gully looking towards Herðubreið. C) Pillow lava sheets (60-100 m thick) are composed of pillow lavas (P11, P12) and associated breccias (B1-B2) exposed in steep sided gully on eastern edge of Austurfjöll. D) Pillow mounds occur in isolation up to 30 m tall and in clusters 15 m tall overlapping other glaciovolcanic deposits.

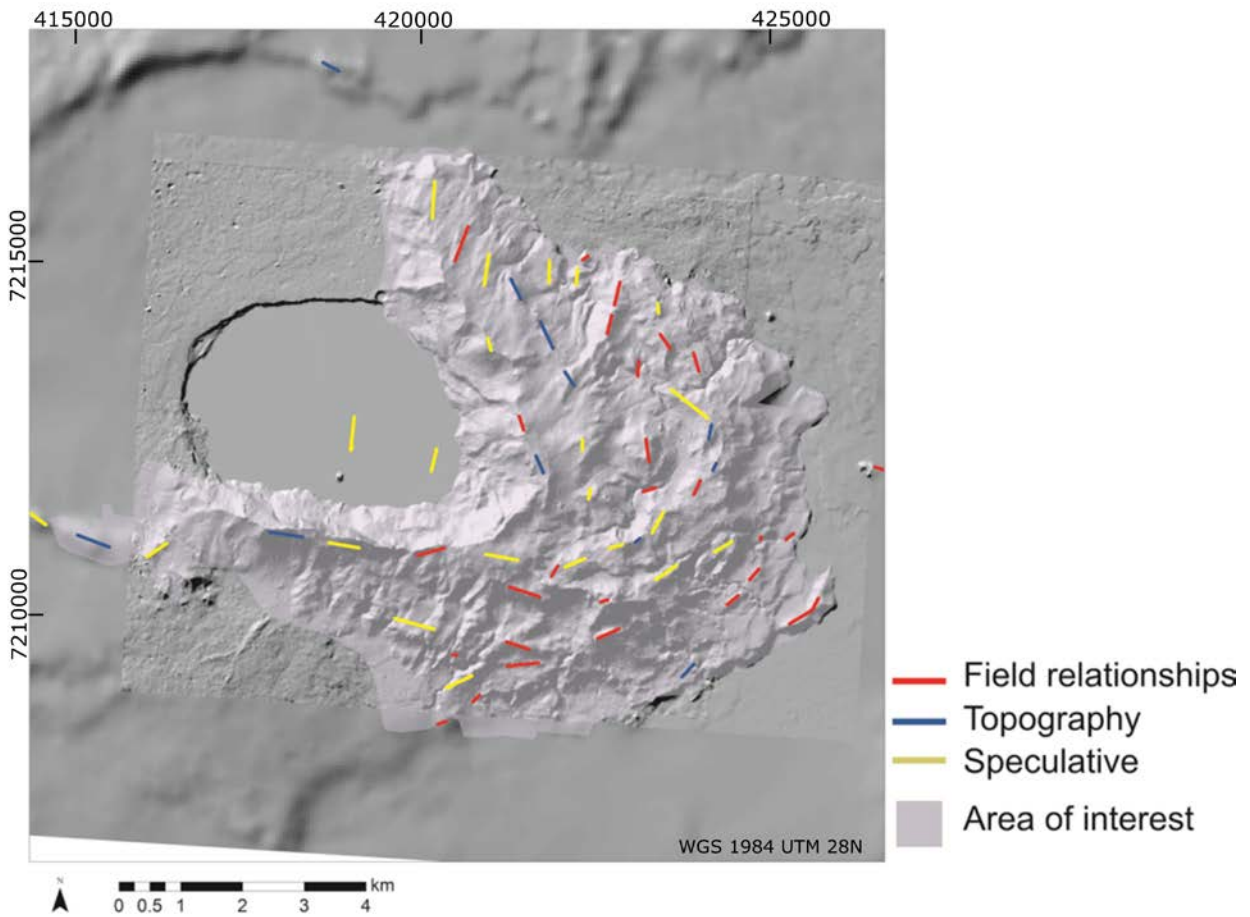


Figure 8: Hillshade produced from a 10 m DEM of Austurfjöll Askja used to indicate vents (predominantly fissure ridges) identified either through field relationships, topography or speculation (incomplete field or topographic evidence). The distribution of the more than 50 surficially exposed vents results in a unique morphology of the massif and neighboring Thorvaldstindur along the southern end of Öskjuvatn.

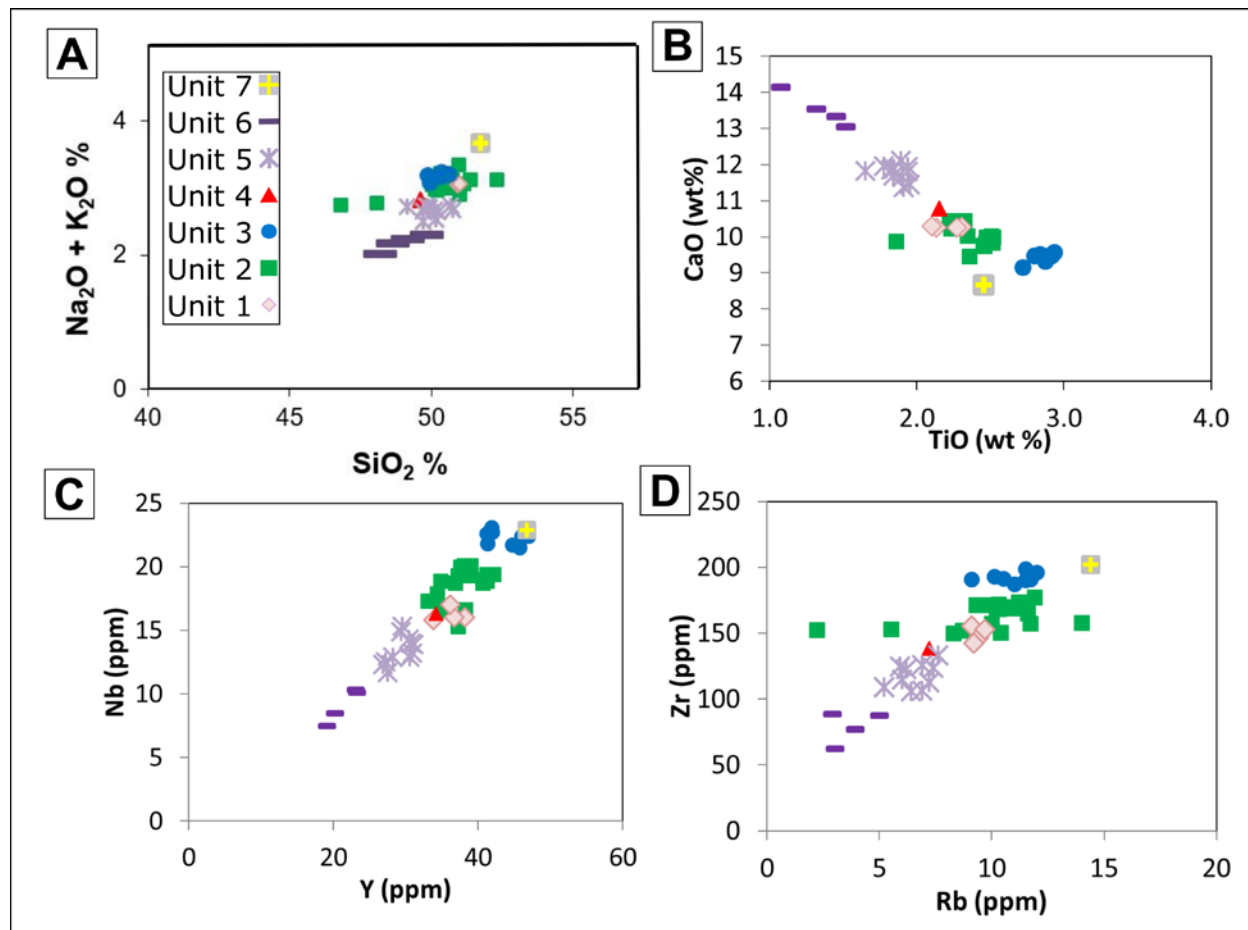


Figure 9: Variation diagrams of Austurfjöll major and trace element geochemistry. Units were initially divided based on stratigraphic relationships, then samples not well constrained by stratigraphy were assigned to a Unit based on trace element geochemistry characteristics of recognized units. A) Total alkali versus silica plot. B) CaO vs. TiO. C- D) Incompatible trace elements Nb vs Y and Zr vs Rb respectively. Incompatible element enrichment trend Unit 6 < Unit 5 < Unit 4 < Unit 1 < Unit 2 < Unit 3 < Unit 7.

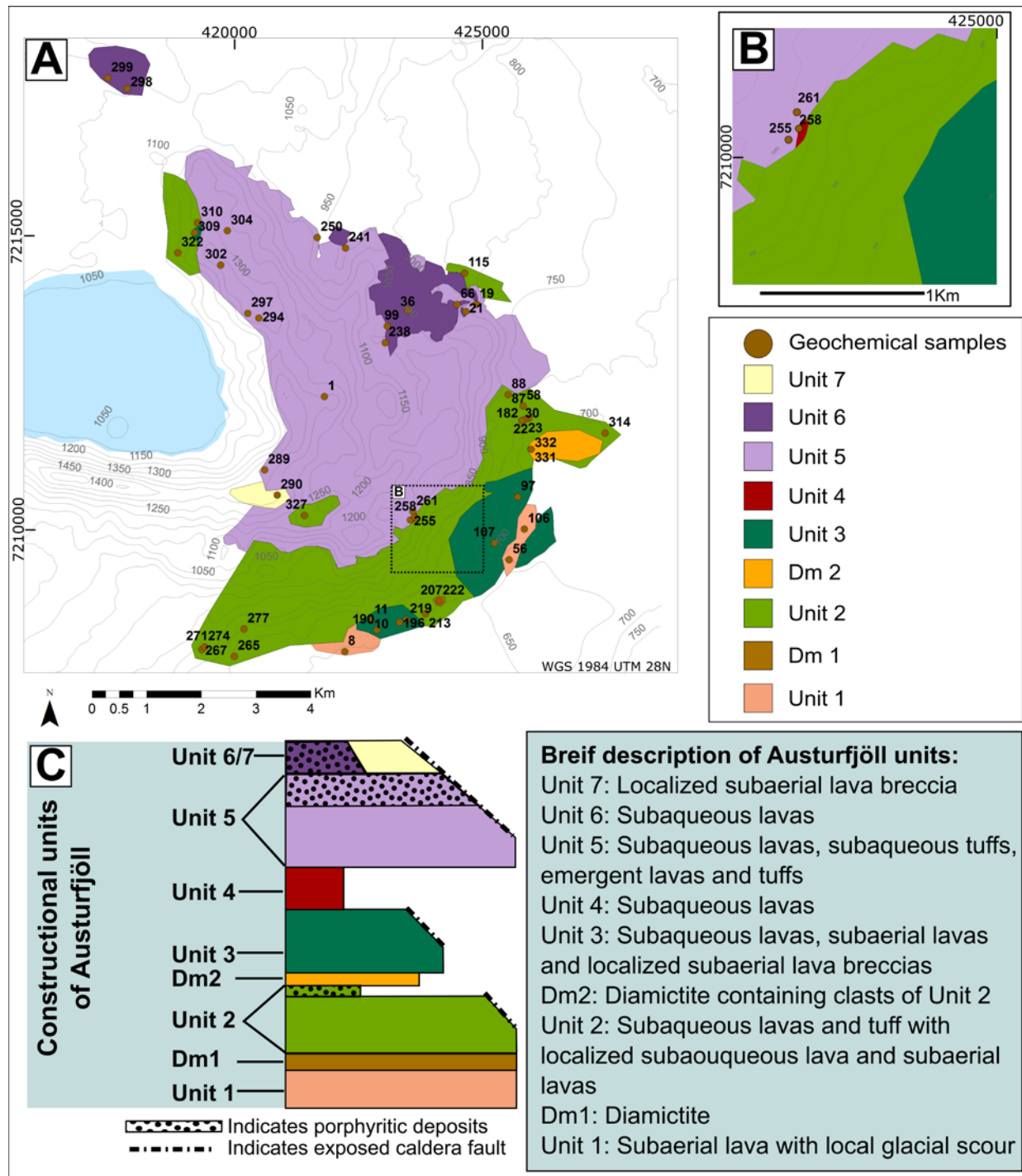


Fig. 10 A) Map of eruptive units at Austurfjöll defined by stratigraphy supplemented with geochemical data. B) Insert region of map to highlight the small exposure of Unit 4. C) Simplified stratigraphic column of the history of the glaciovolcanic massif. Relative width of the column is reflective of unit distribution, while thickness corresponds to unit thickness. The appearance of macro-porphyritic units is noted. The units that are cut by caldera faults are indicated. See Online Resource 2 for cross-sections.

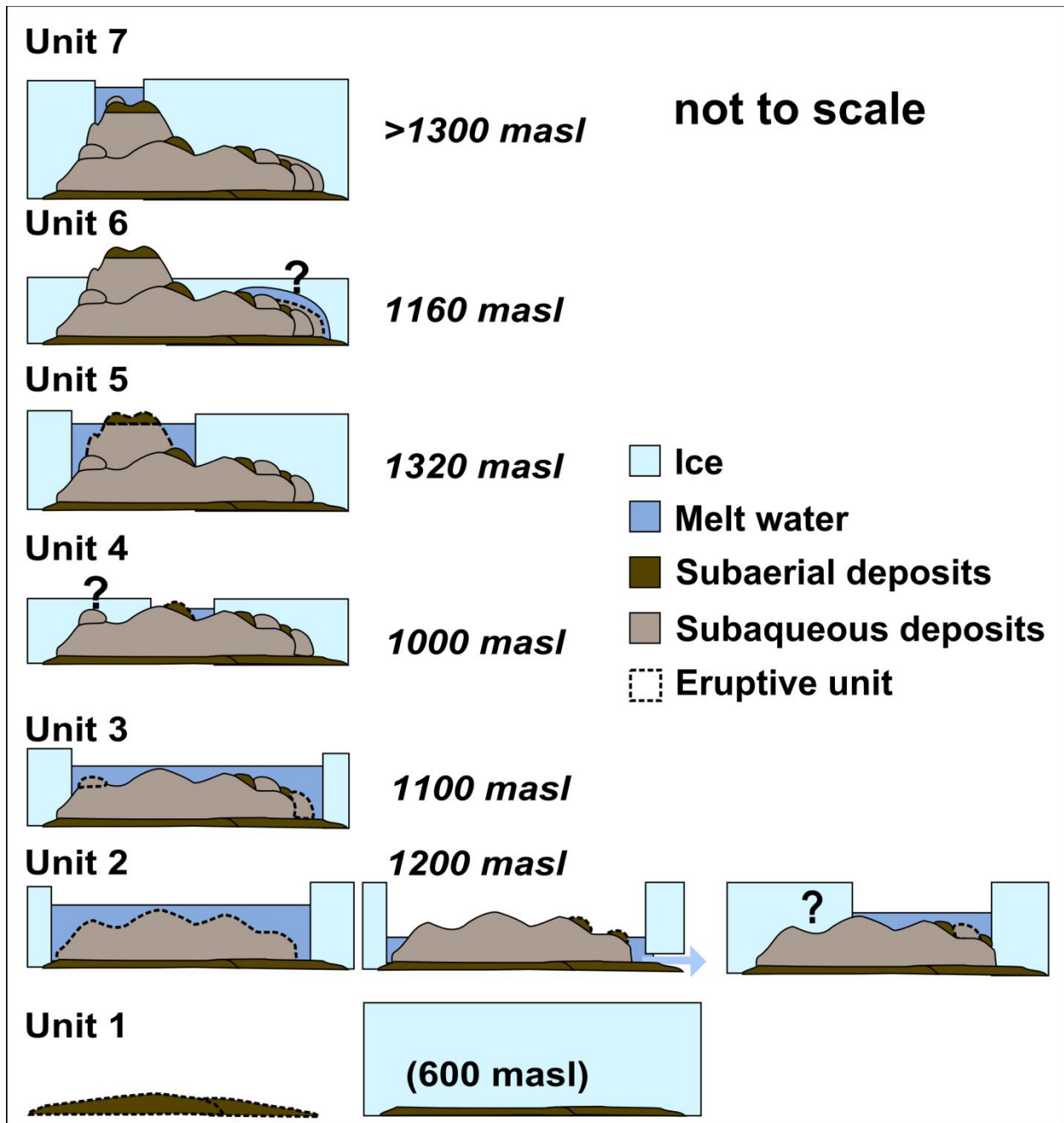


Figure 11: Simplified chronology of relative ice and meltwater positions based on lithofacies mapping and eruptive chronology for Austurfjöll massif using an W-E section. This schematic highlights the variability and recurring nature of meltwater lakes over the massif. The water and ice positions here are minimums, values in italics are maximum elevations of subaqueous deposits for a given unit. Distributions and geometries that involve thicker ice or additional bodies of meltwater are possible. Additional drainage events (as depicted for Unit 2) are also possible. The meltwater is depicted as an open lake due to the large areal extent of the eruptive deposits (Unit 2 & 3). Question marks indicate poorly constrained ice conditions.

Table 1: Lithofacies found at Austurfjöll

Code	General	Description
<i>x= porphyritic</i>		
L	Lavas	
PI₁	Microcrystalline pillows	Regularly stacked pillow forms. Wide range in vesicularity.
PI₂	Microcrystalline pillows	Irregular pillow forms, may have columnar flow cores. Wide range in vesicularity.
PIx₁	Porphyritic pillows	Regular pillow forms. Displays radial and vertical pipe vesicles. Wide range in pillow core. Crystal population dominated by plagioclase, with minor Cpx.
PIx₂	Porphyritic pillows	Irregular pillow forms, may have columnar flow lobes. Wide range in vesicularity. Phenocryst population dominated by plagioclase, with minor Cpx.
L1	Subaqueous sheet lava	Microcrystalline lava, vesicularity is low, can display columnar joints, and chill margins.
Lx	Porphyritic subaqueous sheet lava	Porphyritic lava flow, vesicularity is low. Can display columnar jointing, and chill margins. Phenocryst population dominated by plagioclase, with minor Cpx.
L2	Subaerial lava	Dense, microcrystalline lava with oxidation and local scoriaceous tops.
Lx2	Porphyritic subaerial lava	Dense, microcrystalline lava with oxidation and local scoriaceous tops. Contains visible phenocrysts of plagioclase feldspar. Phenocryst population dominated by plagioclase, with minor Cpx.
B	Breccias	
B1	Microcrystalline pillow breccia	Contains intact pillows and fragments of pillows. Typically angular to subangular. May contain fluidal bombs. Clast to variable clast to matrix support, coarse ash matrix.
Bx1	Porphyritic pillow breccia	Porphyritic pillows and pillow fragments. Phenocryst population dominated by plagioclase, with minor Cpx. Clast to variable clast to matrix support, coarse ash matrix.
B2	Microcrystalline angular block breccia	Contains angular blocks. Clast to variable clast to matrix support, coarse ash matrix.
Bx2	Porphyritic angular block breccia	Porphyritic angular blocks. Phenocryst population dominated by plagioclase, with minor Cpx. Clast to variable clast to matrix support, coarse ash matrix.
B3	Subaerial lava fragment breccia	Fragments of dense subaerial lava. Matrix or clast supported breccia containing coarse ash and lapilli. May include red scoria or porphyritic lithics.
Dia	Diamictite	
Dia1	Matrix supported conglomerate, contains glacial clasts	Subrounded to rounded clasts supported in a fine ash matrix. Distinctive striated cobbles and outsized clasts (glacial erratics). Typically on the order of 1 m thick, but not laterally continuous.
Dia2	Matrix supported	Subrounded to rounded clasts supported in a fine ash

conglomerate matrix. Glacial characteristics like striated clasts may be present. Thin units that are well bedded, dominated by ash sized particles. Typical deposit thickness is on the order of 50 cm and occurs on glacially scoured surfaces.

Lt Lapilli tuffs

- Lt1** Angular glassy lapilli tuff with pillows and fluidal bombs
Dominated by 2-4 cm diameter angular glass fragments, clast or matrix supported with coarse ash matrix. Outsized clasts include pillow fragments and pillow. Massive, normal grading common.
- Lt2** Subrounded lapilli tuff with subangular blocks / bombs no visible phenocrysts
Dominated by subrounded lapilli, clast or matrix supported with outsized clasts of subangular to rounded blocks with a coarse ash matrix. Bedding is inconsistent and weak.
- Lt2x** Porphyritic subrounded lapilli tuff with subangular blocks / bombs
Dominated by subrounded lapilli of porphyritic lava and occasional independent crystals up to 1 cm in diameter. May be clast- or matrix-supported. Outsized clasts include subangular to rounded blocks. Phenocryst population dominated by plagioclase with minor Cpx.
- Lt3** Subaerial component lapilli tuff
Dominated by subrounded lapilli, clast or matrix supported with outsized clasts of bombs and bomb fragments. Coarse ash matrix. Contains armored lapilli, in addition to other subaerial pyroclasts.
- Lt3x** Subaerial porphyritic lapilli tuff
Dominated by subrounded lapilli of porphyritic lapilli sized clasts of lava and independent crystals up to 1 cm in diameter. May be clast or matrix supported. Outsized clasts include lava blocks and bombs. Coarse ash matrix. Contains armored lapilli, in addition to other subaerial pyroclasts.
- Lt4** Heterolithic lapilli tuff
Dominated by 2-4 cm diameter angular lapilli of porphyritic and microcrystalline vesicular clasts. May include red scoria and / or clasts of ash tuff or subaerial lava. Coarse ash matrix supported with outsized clasts of 2-15 cm.

At Ash Tuffs

- At1** Massive coarse ash
Massive coarse ash, with variable palagonitization.
 - At2** Bedded coarse and fine ash, Laminated ash units
Bedded to laminated unit of coarse ash, fine ash, and occasional silt. Laminations occur in beds 2 cm thick.
 - At3** Alternating beds of variable grain sizes dominated by ash
Beds of ash, lapilli and block bearing tuffs. Individual beds range between 2 and 15 cm. Weak sedimentary structures on cm scale, such as ripples and scours may occur.
 - At4** Deformed domains of vitric ash and lapilli
Discrete packets of bedded ash dominated tuffs that have steep dips and convoluted folding that does not match the surrounding bedding. Outsized clasts may range from lapilli to block size.
-

Table 2: Analysis of stratigraphically constrained Unit 2 as a representative of one geochemically distinct magma batch from Austurfjöll (Unit 2).

Unit	2	2	2	2	2	2	2	2	2	2	2	2	2	2	2	2	2	2	2	2	2	2	2	2	Unit	Unit	Analy-
Sample	AG	mean	range	tical																							
	274	331	58	182	22	314	176	207	327	213	30	58a	58b	87	88	115	23	267	322	277	265	310	271			error	
Wt %																											
SiO₂	50.63	50.77	51.13	50.70	50.51	50.64	50.43	51.04	50.43	46.83	50.57	50.13	50.04	51.39	50.23	50.50	50.33	50.46	48.06	52.32	50.33	51.01	50.95	50.41	46.83-52.32	1.00	
TiO₂	2.52	2.50	2.52	2.51	2.49	2.47	2.51	2.28	2.29	2.33	2.48	2.46	2.45	2.50	2.49	2.47	2.51	2.23	2.31	1.86	2.34	2.22	2.36	2.40	1.86-2.52	1.00	
Al₂O₃	13.27	13.22	13.33	13.24	13.22	13.19	13.23	13.76	13.84	13.99	13.31	13.19	13.18	13.37	13.28	13.19	13.25	13.68	14.36	13.94	13.62	14.25	13.69	13.50	13.18-14.29	1.00	
FeO*	14.13	13.87	14.17	14.04	13.79	14.26	14.09	13.50	13.59	13.66	15.79	16.25	16.07	14.83	15.88	15.89	16.06	14.13	13.80	12.14	13.90	12.44	14.20	14.37	12.14-16.25	1.00	
MnO	0.25	0.23	0.24	0.24	0.24	0.24	0.24	0.23	0.24	0.29	0.25	0.25	0.24	0.25	0.25	0.24	0.25	0.24	0.22	0.20	0.24	0.26	0.25	0.24	0.20-0.29	1.00	
MgO	5.22	5.29	5.43	5.37	5.42	5.47	5.00	5.72	5.53	5.21	5.22	5.38	5.39	5.40	5.43	5.46	5.20	5.58	5.18	5.56	5.36	5.45	4.94	5.36	4.94-5.72	1.00	
CaO	10.00	9.92	9.83	9.84	9.95	9.99	9.89	10.40	10.28	10.44	9.95	9.75	9.76	10.03	9.85	9.86	9.92	10.24	10.31	9.87	10.02	10.44	9.46	10.00	9.46-10.44	1.00	
Na₂O	2.52	2.61	2.55	2.59	2.56	2.62	2.58	2.57	2.75	2.56	2.60	2.47	2.52	2.61	2.47	2.54	2.57	2.63	2.41	2.54	2.70	2.51	2.82	2.58	2.41-2.82	1.00	
K₂O	0.48	0.50	0.51	0.49	0.48	0.48	0.48	0.43	0.48	0.19	0.52	0.51	0.53	0.51	0.49	0.54	0.50	0.44	0.37	0.60	0.52	0.38	0.54	0.48	0.19-0.60	1.00	
P₂O₅	0.28	0.27	0.28	0.27	0.27	0.26	0.28	0.24	0.26	0.27	0.28	0.28	0.28	0.28	0.28	0.27	0.28	0.25	0.27	0.21	0.27	0.26	0.29	0.27	0.21-0.29	1.00	
Total ppm	99.3	99.2	99.9	99.3	98.9	99.6	98.7	100.2	99.7	95.8	101.1	100.8	100.6	101.3	100.8	101.1	100.9	99.9	97.3	99.2	99.3	99.2	99.5	99.6			
Nb	19	19	19	19	19	19	19	17	17	18	20	20	20	20	20	19	20	17	18	15	19	19	19	19	17-20	1.00	
Rb	9	11	11	10	11	12	10	9	10	2	11	11	11	11	10	10	10	8	6	14	12	10	12	10	2-14	1.00	
Sr	189	187	186	186	187	183	188	193	214	195	182	178	179	188	181	181	183	201	203	186	214	212	203	191	178-214	1.00	
Y	41	41	42	41	41	41	41	38	33	34	38	38	38	38	38	37	39	35	34	37	35	37	39	38	34-42	1.00	
Zr	172	170	174	172	169	165	172	152	150	153	170	170	169	170	169	169	170	150	153	158	157	157	177	165	150-172	1.00	
Ce	38	39	42	37	39	38	40	32	34	39	56	32	31	36	34	32	57	37	32	34	37	40	36	38	31-57	1.00	
Cu	130	114	119	111	121	127	123	126	131	128	196	214	202	195	208	169	198	127	129	134	140	130	94	146	94-214	0.99	
Ni	36	32	32	31	34	35	32	39	34	31	32	49	45	39	35	33	32	33	33	38	31	30	26	34	26-49	1.00	
Sc	43	43	42	42	41	43	42	43	43	43	42	43	44	45	42	43	41	45	43	38	43	43	41	43	38-45	1.00	
V	424	421	420	417	422	412	424	401	374	390	418	411	409	423	422	418	416	374	378	332	391	367	345	400	332-424	1.00	
Zn	127	128	129	130	125	125	127	118	116	118	98	98	102	115	100	96	100	119	114	105	116	118	125	115	96-130	1.00	

* Total iron measured and reported as FeO. See Online Resource 1.

Analytical error presented is the highest value between the two labs used for this study. See text for detail.

Table 3: Mean composition of eruptive units were first defined by stratigraphic relationships and refined based on chemistry. Incompatible trace elements Nb, Rb, Y, Zr, and Ce were used to establish geochemical fingerprints for eruptive units. In order of increasing enrichment of these incompatible elements: Unit 6, Unit 5, Unit 4, Unit 1, Unit 2, Unit 3 and Unit 7. Trace element ratios highlight the unique combination of concentrations for the units.

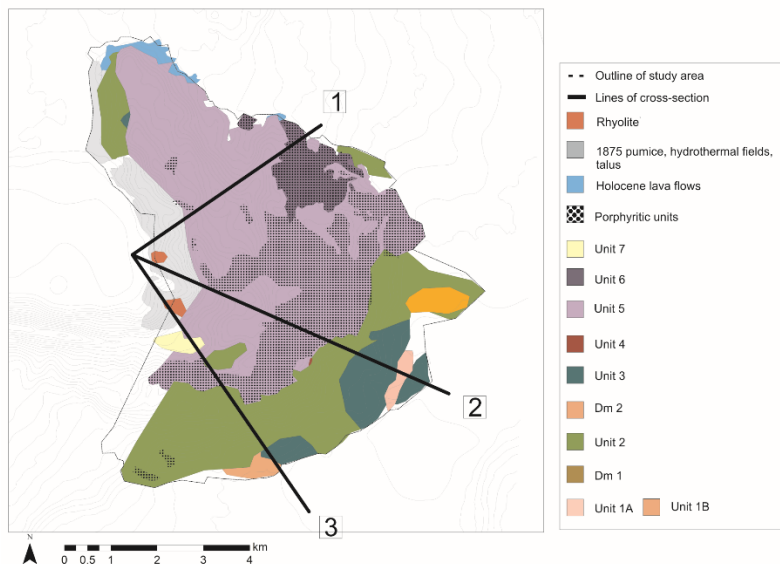
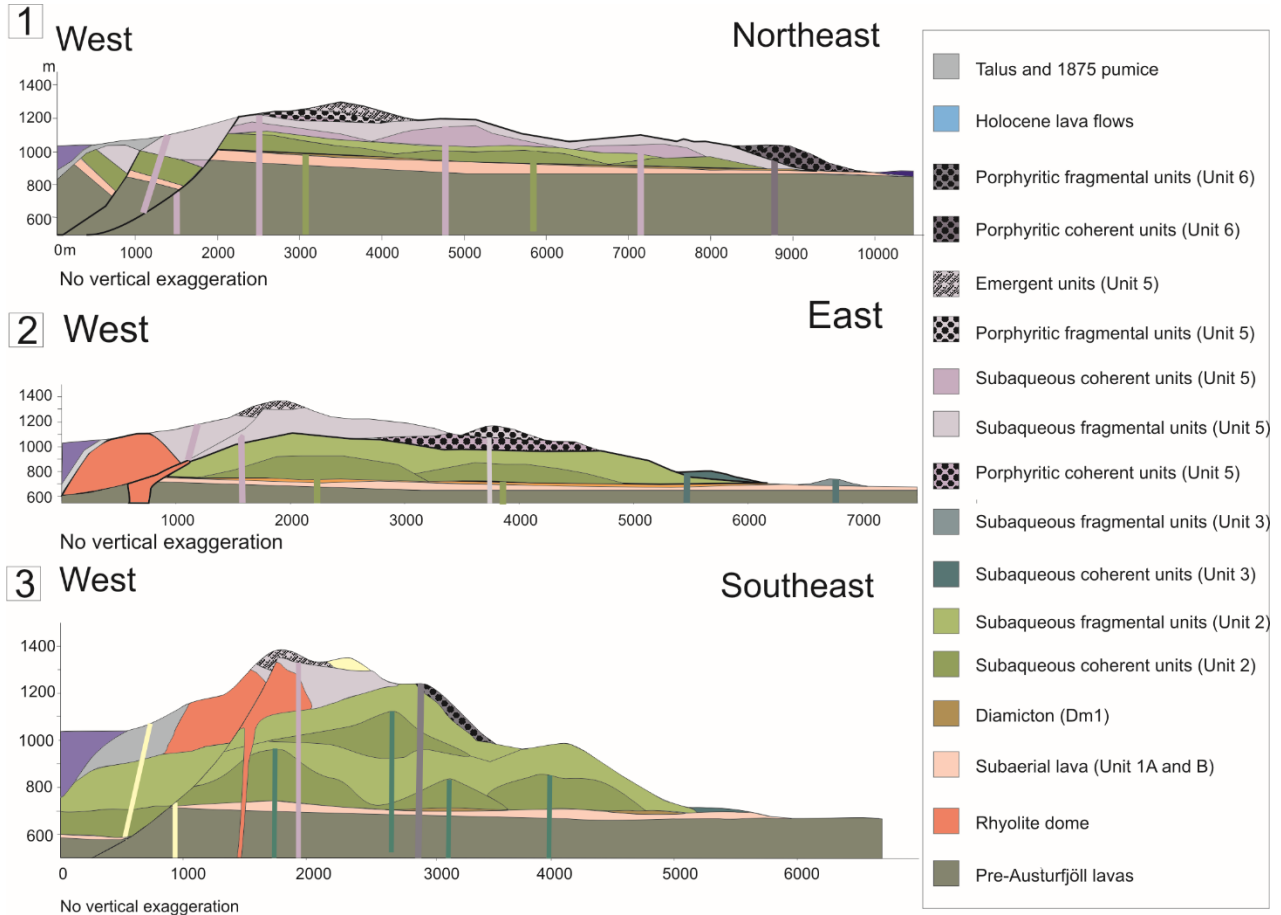
	Unit 1		Unit 2		Unit 3		Unit 4		Unit 5		Unit 6		Unit 7	
	mean	sd	mean	sd	mean	sd	mean	sd	mean	sd	mean	sd	mean	sd
n	4		23		9		1		11		4		1	
wt%														
SiO₂	50.81	0.22	50.41	1.07	50.31	0.25	49.60	-	50.02	0.70	48.96	0.46	51.72	-
TiO₂	2.15	0.10	2.40	0.15	2.85	0.06	2.15	-	1.86	0.20	1.34	0.09	2.45	-
Al₂O₃	13.71	0.03	13.50	0.37	13.00	0.17	13.60	-	14.74	1.32	19.08	1.03	14.13	-
FeO*	14.30	0.85	14.37	1.13	15.61	0.81	13.94	-	11.90	0.80	8.92	0.79	13.26	-
MnO	0.23	0.00	0.24	0.02	0.25	0.00	0.24	-	0.21	0.01	0.17	0.02	0.23	-
MgO	5.73	0.03	5.36	0.18	4.98	0.12	5.92	-	6.05	0.82	4.78	0.86	3.70	-
CaO	10.37	0.02	10.00	0.25	9.42	0.13	10.79	-	11.78	0.46	13.52	0.22	8.67	-
Na₂O	2.60	0.00	2.58	0.09	2.68	0.04	2.47	-	2.35	0.07	2.00	0.07	2.99	-
K₂O	0.44	0.02	0.48	0.08	0.51	0.06	0.35	-	0.31	0.04	0.19	0.03	0.70	-
P₂O₅	0.23	0.01	0.27	0.02	0.33	0.00	0.23	-	0.20	0.02	0.13	0.01	0.34	-
Total	100.7		99.6		100.0		99.3		99.4		99.1		98.2	
ppm														
Nb	16	0.5	19	1.3	22	0.5	16	-	13	1.3	9	1.1	23	-
Rb	9	0.3	10	2.3	11	0.9	7	-	6	1.0	4	0.8	14	-
Sr	192	3.4	191	11.1	192	6.8	195	-	205	7.3	221	9.6	215	-
Y	35	1.8	38	2.6	44	2.2	34	-	29	2.1	21	1.6	47	-
Zr	145	5.9	165	8.6	193	3.4	139	-	117	12.0	79	9.3	202	-
Ce	38	13.5	38	6.6	43	3.4	31	-	26	1.5	19	3.2	49	-
Cu	180	48.4	146	36.4	138	28.4	137	-	157	22.3	119	26.4	107	-
Ni	35	4.3	34	5.0	29	1.9	32	-	46	5.2	41	10.8	20	-
Sc	43	0.8	43	1.5	42	1.9	45	-	45	3.3	37	3.0	41	-
V	392	9.5	400	26.8	456	13.1	387	-	335	26.1	251	24.8	335	-
Zn	99	18.3	115	11.4	127	15.1	115	-	96	10.1	70	7.4	167	-
Rb/Nb	0.57		0.54		0.50		0.44		0.47		0.41		0.61	
Zr/Nb	9.18		8.79		8.61		8.69		8.72		8.51		8.78	
Y/Nb	2.22		2.03		1.96		2.13		2.18		2.30		2.04	

*Total iron measured and reported as FeO.

Table 4: Key features and significance of eruptive units described at Austurfjöll, Askja, Iceland

Eruptive unit	Facies	Unique properties	Implications
7	B3	Isolated with no obvious source, subaqueous and subaerial components	Vent was located in area of modern calderas
6	Plx1, Plx2, Ltx2, Atx2	Exclusively porphyritic and subaqueous	Subaqueous activity continued after emergence
5	PI1, PI2, Plx1, Plx2, L1, L2, Lx1, B1-3, B1x, Lt1-4, At1-4, G1	Contains diverse componentry, including xenoliths, red scoria, and coated lapilli. G1, B3, Lt4	Records both subaqueous and emergent activity
4	PI2	Mega pillows, isolated	Limited exposure: burial, or limited eruption
3	PI1, PI2, L1, L2, B1-2, Lt1-2, At1-4	Limited distribution	Mantling paleotopography
2	PI1, Plx1, PI2, L2, B1, Lt1-2, At1-3, Dia1	Voluminous pillow sheets	First subaqueous Austurfjöll unit
1	L2, Dia1 , Dia2	Subaerial lava only Glacial scour	Pre-glacial advance

Online resource 1: Complete geochemical dataset (excel spreadsheet).



Online resource 2: Example cross-sections through the Austurkjöll massif indicating the development of massif as a sequence of fissure fed pillow lava sheets followed by more explosive fissure ridges. The position of the rhyolite dome is poorly constrained. The position noted here is controlled by exposures and the lack of deformation in over lying unit. The exposures of rhyolite in section 2 and 3 may represent one large deposit or two isolated deposits.